J|A|C|S
ARTICLES
Published on Web 07/17/2003

Efficient Excitation Energy Transfer in Long *Meso*−*Meso* Linked Zn(II) Porphyrin Arrays Bearing a 5,15-Bisphenylethynylated Zn(II) Porphyrin Acceptor

Naoki Aratani,[†] Hyun Sun Cho,[‡] Tae Kyu Ahn,[‡] Sung Cho,[‡] Dongho Kim,*[,‡] Hitoshi Sumi,*[,§] and Atsuhiro Osuka*[,†]

Contribution from the Department of Chemistry, Graduate School of Science, Kyoto University, and Core Research for Evolutional Science and Technology (CREST), Japan Science and Technology Corporation, Sakyo-ku, Kyoto 606-8502, Japan, Center for Ultrafast Optical Characteristics Control and Department of Chemistry, Yonsei University, Seoul 120-749, Korea, and Institute of Materials Science, University of Tsukuba, Tsukuba 305-8573, Japan

Received January 3, 2003; E-mail: osuka@kuchem.kyoto-u.ac.jp

Abstract: Electronically coupled porphyrin arrays are suitable for artificial light harvesting antenna in light of a large absorption cross-section and fast excitation energy transfer (EET). Along this line, an artificial energy transfer model system has been synthesized, comprising of an energy donating *meso*−*meso* linked Zn(II) porphyrin array and an energy accepting 5,15-bisphenylethynylated Zn(II) porphyrin linked via a 1,4-phenylene spacer. This includes an increasing number of porphyrins in the *meso*−*meso* linked Zn(II) porphyrin array, 1, 2, 3, 6, 12, and 24 (**Z1A**, **Z2A**, **Z3A**, **Z6A**, **Z12A**, and **Z24A**). The intramolecular singlet−singlet EET processes have been examined by means of the steady-state and time-resolved spectroscopic techniques. The steady-state fluorescence comes only from the acceptor moiety in **Z1A**−**Z12A**, indicating nearly the quantitative EET. In **Z24A** that has a molecular length of ca. 217 Å, the fluorescence comes largely from the acceptor moiety but partly from the long donor array, indicating that the intramolecular EET is not quantitative. The transient absorption spectroscopy has provided the EET rates in real time scale: $(2.5\ \text{ps})^{-1}$ for **Z1A**, $(3.3\ \text{ps})^{-1}$ for **Z2A**, $(5.5\ \text{ps})^{-1}$ for **Z3A**, $(21\ \text{ps})^{-1}$ for **Z6A**, $(63\ \text{ps})^{-1}$ for **Z12A**, and $(108\ \text{ps})^{-1}$ for **Z24A**. These results have been well explained by a revised Förster equation (Sumi formula), which takes into account an exciton extending coherently over several porphyrin pigments in the donor array, whose length is not much shorter than the average donor−acceptor distance. Advantages of such strongly coupled porphyrin arrays in light harvesting and transmission are emphasized in terms of fast EET and a large absorption cross-section for incident light.

Introduction

Photosynthesis starts by the absorption of a photon by light-harvesting (antenna) complexes that usually comprise of a large number of pigments embedded in protein matrixes.[1] This process is followed by a rapid and an efficient energy migration over many pigments within the antenna system until a reaction center is encountered, where photoinduced charge separation takes place for fixation of the solar energies harvested. Photosynthetic organisms often utilize electronically coupled chromophores to capture dilute sunlight as well as enhance the energy transfer efficiency as seen in chlorosomes[2] and LH1[3a] and LH2[3b,c] in bacterial antenna systems and in phycobilisomes in cyanobacteria and red algae.[4] In these cases, photosynthetic pigments form aggregates whose excitation leads to the formation of excitons with quantum-mechanical coherence extending over many chromophores.

Numerous artificial molecular architectures based on porphyrins have been explored with the aim of achieving efficient and directed energy transfer.[5,6] Although some of these studies help understand light-harvesting and energy-transfer phenomena at the molecular level, there is only a limited number of reports on the energy transfer system involving a strongly coupled array of donor or acceptor.[7] Strong electronic coupling (exciton coupling) leads to the alteration of the absorption and emission properties, hence affecting the EET efficiency. More impor-

[†] Kyoto University.
[‡] Yonsei University.
[§] University of Tsukuba.

(1) (a) van Grondelle, R.; Dekker, J. P.; Gillbro, T.; Sundström, V. *Biochim. Biophys. Acta* **1994**, *1187*, 1. (b) Pullerits, T.; Sundström, V. *Acc. Chem. Res.* **1996**, *29*, 381.
(2) (a) Blankenship, R. E.; Olson, J. M.; Miller, M. In *Anoxygenic Photosynthetic Bacteria*; Blankenship, R. E., Madigan, M. T., Bauer, C. E., Eds.; Kluwer Academic Publishers: The Netherlands, 1995; p 399. (b) Holzwarth, A. R.; Griebenow, K.; Shaffner, K. *J. Photochem. Photobiol. A* **1992**, *65*, 61. (c) Hildebrandt, P.; Tamiaki, H.; Holzwarth, A. R.; Shaffner, K. *J. Phys. Chem.* **1994**, *98*, 2192.
(3) (a) Karrasch, S.; Bullough, P. A.; Ghosh, R. *EMBO J.* **1995**, *14*, 631. (b) McDermott, G.; Prince, S. M.; Freer, A. A.; Hawthornthwaite-Lawless, A. M.; Papiz, M. Z.; Cogdell, R. J.; Isaacs, N. W. *Nature* **1995**, *374*, 517. (c) Koepke, J.; Hu, X.; Muenke, C.; Schulten, K.; Michel, H. *Structure* **1996**, *4*, 581.
(4) (a) Gantt, E. *Int. Rev. Cytol.* **1980**, *66*, 45. (b) Yamazaki, I.: Mimuro, M.; Tamai, N.; Yamazaki, T.; Fujita, Y. *Photochem. Photobiol.* **1984**, *39*, 233. (c) Holzwarth, A. R.; Wendler, J.; Suter, G. W. *Biophys. J.* **1987**, *51*, 1.
(5) (a) Wasielewski, M. R. *Chem. Rev.* **1992**, *92*, 435. (b) Gust, D.; Moore, T. A.; Moore, A. L. *Acc. Chem. Res.* **1993**, *26*, 198. (c) Gust, D.; Moore, T. A.; Moore, A. L. *Acc. Chem. Res.* **2001**, *34*, 40. (d) Holten, D.; Bocian, D. F.; Lindsey, J. S. *Acc. Chem. Res.* **2002**, *35*, 57.

 10.1021/ja030002u CCC: $25.00

tantly, unless forming a stacked nonfluorescent energy sink, an electronically coupled array of chromophores may be favorable for the light harvesting antenna function owing to faster interporphyrin energy hopping and a larger absorption cross-section. Such effects have been only scarcely tested in structurally well-defined synthetic models.

The peripheral antenna LH2 of the photosynthetic purple bacteria forms two wheel-like structures with 9 bacteriochlorophyll (Bchl) *a* molecules (B800) and 18 Bchl *a* molecules (B850).[4a] While Bchl *a* molecules in B800 are electronically weakly interacting with each other, those in B850 are electronically strongly coupled, causing the exciton states, due to a close face-to-face arrangement with an Mg−Mg distance of 8.7 Å. EET takes place very rapidly from B800 to B850 within a time of 0.7−0.9 ps at room temperature.[1] When a strict 9-fold symmetry is assumed for B850, optically allowed is only the second lowest exciton state with the lowest exciton state becoming dipole-forbidden.[8] In this situation, it would be difficult to explain the very rapid energy transfer from B800 to B850 within a framework of Förster mechanism, which allows EET only between optically allowed states. The energy-accepting optically allowed state in B850 is located too low from the energy donating B800 state. This optically forbidden lowest exciton state in B850 may be involved in the subsequent EET to LH1 as an energy donor. Recently, Sumi proposed a revised Förster formula for EET[8] that occurs between a donor and an acceptor in a situation where at least one of them is an exciton holding aggregate of chromophores. When the physical size of aggregate is not much smaller than the average donor−acceptor distance, as found quite commonly in natural photosynthetic systems, individual chromophores retain their transition dipoles against the EET partner, even if their overall sum is nearly zero due to the dipole-forbidden nature of an exciton state.[8] This revised formula has explained the rapid EET from B800 to B850 in a satisfactory manner.[9]

Here, we report the synthesis and EET processes of covalently linked donor−acceptor systems, **Z*n*A**; $n = 1, 2, 3, 6, 12,$ and 24, as shown in Schemes 1−3, in which a 5,15-bisphenylethynylated porphyrin acceptor is linked via a 1,4-phenylene spacer at the end *meso*-carbon of a *meso*−*meso* linked Zn(II) porphyrin array. Recently, we reported the synthesis of extremely long, yet discrete *meso*−*meso* linked porphyrin arrays by Ag(I)-promoted oxidative coupling.[10,11] A key feature of these porphyrin arrays is the good solubility in many organic solvents including THF and $CHCl_3$. Therefore, despite the large molecular size, these molecules can be separated, purified, and subjected to many chemical reactions in a manner similar to those of normal organic molecules. *Meso*−*meso* linked porphyrin arrays thus prepared have two free *meso*-positions, which

Scheme 1. Synthesis of **Z2A**[a]

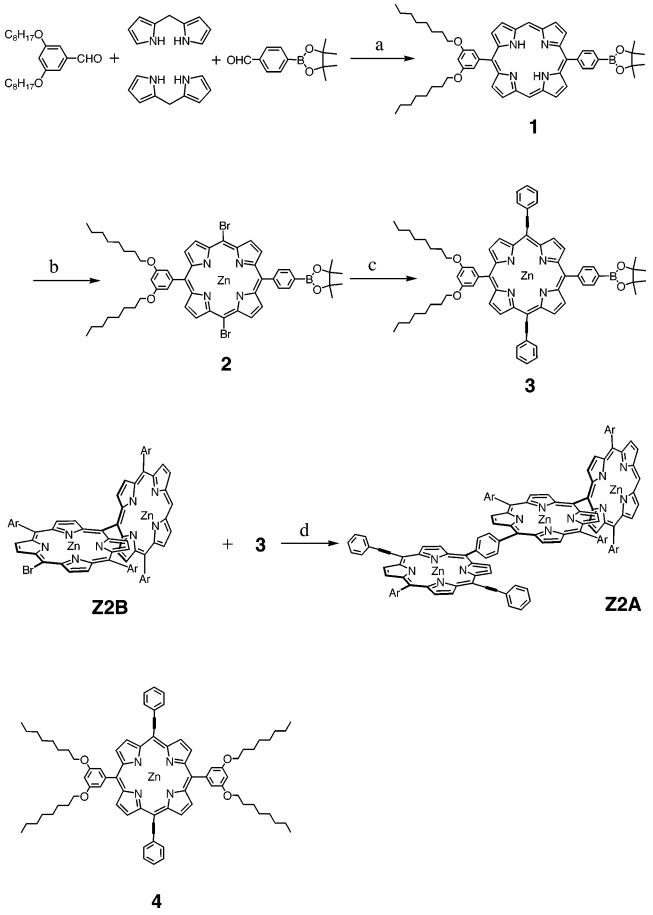

[a] Ar = 3,5-dioctyloxyphenyl. Conditions: (a) (i) TFA, (ii) DDQ, 13%; (b) (i) NBS, pyridine, CH_2Cl_2, (ii) $Zn(OAc)_2$, 92%; (c) phenylacetylene, CuI, $PdCl_2(PPh_2)_2$, triethylamine, toluene, 64%; (d) $Pd(Ph_3)_4$, Cs_2CO_3, DMF, toluene, 76%.

(6) (a) Dubowchik, G. M.; Hamilton, A. D. *J. Chem. Soc., Chem. Commun.* **1987**, 293. (b) Osuka, A.; Maruyama, K.; Yamazaki, I.; Tamai, N. *Chem. Phys. Lett.* **1990**, *165*, 392. (c) Sessler, J. L.; Capuano, V. L.; Harriman, A. *J. Am. Chem. Soc.* **1993**, *115*, 4618. (d) Wagner, R. W.; Lindsey, J. S. *J. Am. Chem. Soc.* **1994**, *116*, 9759. (e) Osuka, A.; Tanabe, N.; Kawabata, S.; Yamazaki, I.; Nishimura, Y. *J. Org. Chem.* **1995**, *60*, 7177. (f) Officer, D. L.; Burrell, A. K.; Reid, D. C. W. *Chem. Commun.* **1996**, 1657. (g) Osuka, A.; Tanabe, N.; Nakajima, S.; Maruyama, K. *J. Chem. Soc., Perkin Trans. 2* **1996**, 199. (h) Jensen, K. K.; van Berlekom, S. B.; Kajanus, J.; Martensson, J.; Albinsson, B. *J. Phys. Chem. A.* **1997**, *101*, 2218. (i) Taylor, P. L.; Wylie, A. P.; Huuskonen, J.; Anderson, H. L. *Angew. Chem., Int. Ed.* **1998**, *37*, 986. (j) Mongin, O.; Papamicaël, C.; Hoyler, N.; Gossauer, A. *J. Org. Chem.* **1998**, *63*, 5568. (k) Nakano, A.; Osuka, A.; Yamazaki, I.; Yamazaki, T.; Nishimura, Y. *Angew. Chem., Int. Ed.* **1998**, *37*, 3023. (l) Biemans, H. A. M.; Rowan, A. E.; Verhoeven, A.; Vanoppen, P.; Latterini, L.; Foekema, J.; Schenning, A. P. H. J.; Meijer, E. W.; De Schryver, F. C.; Nolte, R. J. M. *J. Am. Chem. Soc.* **1998**, *120*, 11054. (m) Sugiura, K.; Tanaka, H.; Matsumoto, T.; Kawai, T.; Sakata, Y. *Chem. Lett.* **1999**, 1193−1194. (n) Yeow, E. K. L.; Ghiggino, K. P.; Reek, J. N. H.; Crossley, M. J.; Bosman, A. W.; Schenning, A. P. H. J.; Meijer, E. W. *J. Phys. Chem. B* **2000**, *104*, 2596. (o) Benites, M. R.; Johnson, T. E.; Weghorn, S.; Yu, L.; Rao, P. D.; Diers, J. R.; Yang, S. I.; Kirmaier, C.; Bocian, D. F.; Holten, D.; Lindsey, J. S. *J. Mater. Chem.* **2001**, *12*, 65. (p) Nakano, A.; Osuka, A.; Yamazaki, T.; Nishimura, Y.; Akimoto, S.; Yamazaki, I.; Itaya, A.; Murakami, M.; Miyasaka, H. *Chem.—Eur. J.* **2001**, *7*, 3134. (q) Choi, M.-S.; Aida, T.; Yamazaki, T.: Yamazaki, I. *Chem.—Eur. J.* **2002**, *8*, 668.
(7) Tamiaki, H.; Miyatake, T.; Tanikaga, R.; Holzwarth, A. R.; Shaffner, K. *Angew. Chem., Int. Ed. Engl.* **1996**, *35*, 772.
(8) (a) Sumi, H. *J. Phys. Chem. B* **1999**, *103*, 252. (b) Sumi, H. *J. Luminesc.* **2000**, *87*−*89*, 71. (c) Sumi, H. *Chem. Record* **2001**, *1*, 480.
(9) (a) Mukai, K.; Abe, S.; Sumi, H. *J. Phys. Chem. B* **1999**, *103*, 6096. (b) Mukai, K.; Abe, S.; Sumi, H. *J. Luminesc.* **2000**, *87*−*89*, 818. (c) Scholes, G. D.; Fleming, G. R. *J. Phys. Chem. B* **2000**, *104*, 1854. (d) Scholes, G. D.; Jordanides, X. J.; Fleming, G. R. *J. Phys. Chem. B* **2001**, *105*, 1640.
(10) (a) Osuka, A.; Shimidzu, H. *Angew. Chem., Int. Ed. Engl*. **1997**, *36*, 135. (b) Aratani, N.; Osuka, A.; Kim, Y. H.; Jeong, D. H.; Kim, D. *Angew. Chem., Int. Ed.* **2000**, *39*, 1458. (c) Kim, Y. H.; Jeong, D. H.; Kim, D.; Jeoung, S. C.; Cho, H. S.; Kim, S. K.; Aratani, N.; Osuka, A. *J. Am. Chem. Soc.* **2001**, *123*, 76. (d) Nakano, A.; Yamazaki, T.; Nishimura, Y.; Yamazaki, I.; Osuka, A. *Chem.—Eur. J.* **2000**, *6*, 3254. (e) Yoshida, N.; Aratani, N.; Osuka, A. *Chem. Commun*. **2000**, 197. (f) Piet, J. J.; Taylor, P. N.; Anderson, H. L.; Osuka, A.; Warman, J. M. *J. Am. Chem. Soc*. **2000**, *122*, 1749. (g) Yoshida, N.; Osuka, A. *Org. Lett*. **2000**, *2*, 2963.
(11) (a) Susumu, K.; Shimidzu, T.; Tanaka, K.; Segawa, H. *Tetrahedron Lett*. **1996**, *37*, 8399. (b) Khoury, R. G.; Jaquinod, L.; Smith, K. M. *Chem. Commun*. **1997**, 1057. (c) Senge, M. O.; Feng, X. *Tetrahedron Lett*. **1999**, *40*, 4165. (d) Wojaczynski, J.; Latos-Grazynski, L.; Chmielewski, P. J.; Van Calcar, P.; Balch, A. L. *Inorg. Chem*. **1999**, *38*, 3040. (e) Shi, X.; Liebeskind, L. S. *J. Org. Chem*. **2000**, *65*, 1655. (e) Miller, M. A.; Lammi, R. K.; Prathapan, S.; Holten, D.; Lindsey, J. S. *J. Org. Chem*. **2000**, *65*, 6634. (f) Ogawa, K.; Kobuke, Y. *Angew. Chem., Int. Ed.* **2000**, *39*, 4070. (g) Imahori, H.; Tamaki, K.; Araki, Y.; Sekiguchi, Y.; Ito, O.; Sakata, Y.; Fukuzumi, S. *J. Am. Chem. Soc*. **2002**, *124*, 5165. (h) Bonifazi, D.; Diederich, F. *Chem. Commun*. **2002**, 2178.

Scheme 2. Molecular Structures of **Z1A**−**Z12A**[a]

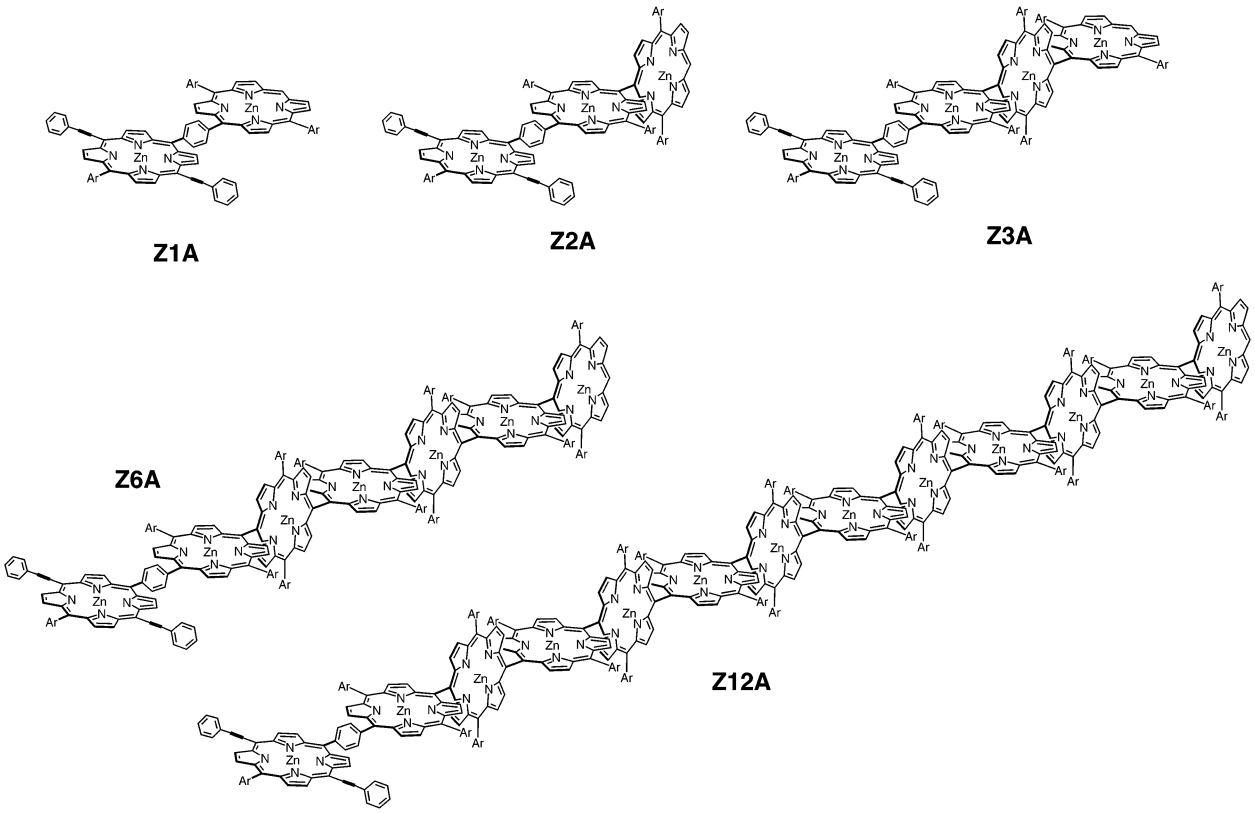

[a] Ar = 3,5-dioctyloxyphenyl.

Scheme 3. Molecular Structure of **Z24A**[a]

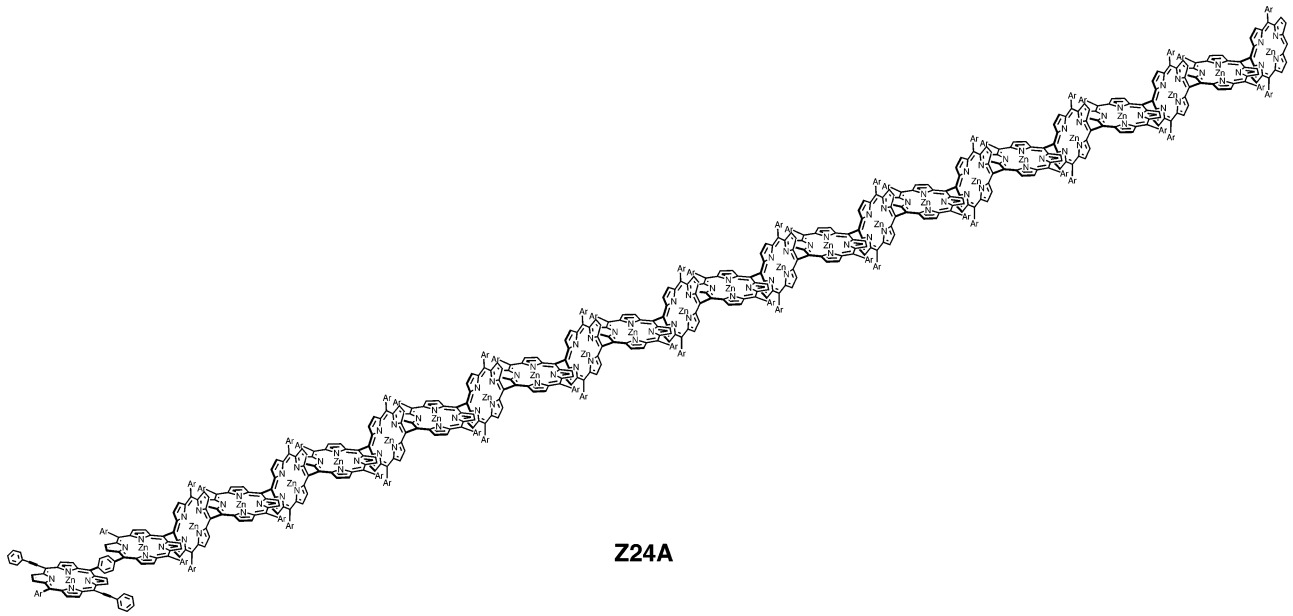

[a] Ar = 3,5-dioctyloxyphenyl.

are used for the attachment of the energy acceptor. Another interesting feature is the direct *meso*−*meso* linkage, which gives rise to substantially large electronic coupling, but the resultant orthogonal conformation of the neighboring porphyrins disrupts the electronic π-conjugation.[10c,f] These properties may be favorable for achieving efficient energy transfer along the array. In addition, the restricted linear geometry of *meso*−*meso* linked porphyrin arrays avoids the formation of a stacked dimeric energy sink that might disrupt the energy-transfer flow along the array. The linear geometry is also interesting with regard to the topological effect on antenna function.[12] With this background, we have examined the excitation energy transfer in **Z*n*A**.

Molecular Design and Synthesis. Scheme 1 shows the synthetic route. *Meso*-*meso* linked Zn(II) porphyrin arrays **Z2**, **Z3**, **Z6**, **Z12**, and **Z24** were synthesized by the usual Ag^{I}-

(12) Van Patten, P. G.; Shreve, A. P.; Lindsey, J. S.; Donohoe, R. *J. Phys. Chem. B* **1998**, *102*, 4209.

promoted coupling of 5,15-diaryl Zn(II) porphyrin **Z1**.[10a−e] Controlled NBS bromination of **Z1**, **Z2**, **Z3**, **Z6**, **Z12**, and **Z24** gave a mixture of *meso*-bromo- and *meso*,*meso*′-dibromo Zn(II) porphyrins. The *meso*-monobrominated porphyrins, **Z1B**, **Z2B**, **Z3B**, **Z6B**, **Z12B**, and **Z24B**, were coupled with boronate Zn(II) porphyrin **3** under Suzuki coupling conditions to furnish **Z1A**, **Z2A**, **Z3A**, **Z6A**, **Z12A**, and **Z24A**, respectively. These model compounds have *meso*−*meso* linked Zn(II) porphyrin arrays as the energy donor and a 5,15-bisphenylethynylated Zn(II) porphyrin[13] as the energy acceptor. The latter has been shown to act as an energy acceptor owing to its red-shifted Q-band and hence favorable spectral overlap for the energy transfer from the *meso*−*meso* linked porphyrin array.[14]

Results

Synthesis. *p*-(4,4,5,5-Tetramethyl-1,3,2-dioxaborolan-2-yl)-benzaldehyde was prepared in 92% yield by pinacol protection of 4-formylphenylboronic acid. The porphyrin boronate **1** was prepared in 13% yield from the acid-catalyzed condensation of 3,5-dioctyloxybenzaldehyde[10b] and the protected boronate with 2.0 equiv of 2,2′-dipyrromethane followed by oxidation with 3 equiv of DDQ.[15,16] Subsequent bromination of **1** with 2.2 equiv of NBS followed by zinc metalation yielded Zn(II) dibromoporphyrin **2** in 92% yield. Sonogashira coupling of the porphyrin **2** with an excess of phenylacetylene (bis(triphenylphosphine) palladium(II) chloride and CuI, triethylamine/toluene, at 50 °C, for 3 h) gave 5,15-bisphenylethynylated boronate Zn(II) porphyrin **3** in 64% yield.[14,17] Finally, Suzuki cross-coupling reaction of the porphyrin **3** with **Z1B**, **Z2B**, **Z3B**, **Z6B**, **Z12B**, and **Z24B** (10 mol % $Pd(PPh_3)_4$, 3 equiv Cs_2CO_3, DMF/toluene, at 80 °C, for 4 h) gave models **Z1A**, **Z2A**, **Z3A**, **Z6A**, **Z12A**, and **Z24A** in 10−77% yields.[18] Models **Z*n*A** were difficult to separate over the usual silica gel column but were obtained in a pure form by using the recycling preparative GPC−HPLC. In the case of **Z24A**, as many as 16 recycling separations over our GPC−HPLC setup enabled the isolation of pure **Z24A** in 28% (Supporting Information I). 5,15-Bisphenylethynyl-10,20-bis(3,5-dioctyloxyphenyl) Zn(II) porphyrin **4** was prepared as a reference molecule.[14b] All new compounds were fully characterized by ^{1}H NMR spectra, FAB or MALDI-TOF mass spectroscopy, UV−vis absorption spectroscopy, and GPC analysis. Among these, the long porphyrin arrays **Z12A** and **Z24A** contain 13 and 25 porphyrin units in a linear fashion with a molecular length of 113 and 217 Å, respectively. The corresponding parent ions were clearly detected at $m/e = 13\,423$ (calcd for $C_{832}H_{1044}N_{52}O_{50}Zn_{13}$, 13 423.9) and $m/e = 25\,862$ (calcd for $C_{1600}H_{2028}N_{100}O_{98}Zn_{25}$, 25 865.1) in the MALDI-TOF mass spectra (Figure 1).

Steady-State Spectra. Figure 2 shows the absorption spectra of **Z1A**, **Z2A**, **Z3A**, **Z6A**, **Z12A**, and **Z24A** in THF, along with those of 1:1 mixtures of acceptor-free *meso*−*meso* linked porphyrin arrays (**Z1**, **Z2**, **Z3**, **Z6**, **Z12**, and **Z24**) and the porphyrin **4**. In line with the previous studies,[10] the exciton-split Soret bands of the *meso*−*meso* linked porphyrin arrays are observed at 417−423 nm and at >466 nm. The Soret bands of the bisphenylethynylated Zn(II) porphyrin are observed constantly at 448 nm. The Q-bands of the *meso*−*meso* linked porphyrin arrays are observed at 550−588 nm with progressive intensification and red shift upon the increase of the number of porphyrins, while the Q-bands of the bisphenylethynylated Zn(II) porphyrin are observed at 649 nm. Comparisons of the respective absorption spectra revealed that the absorption spectra of **Z*n*A** in the Q-band region are essentially given by the sum of the spectra of *meso*−*meso* linked porphyrin arrays **Z*n*** and **4**, indicating that electronic interactions in the ground state are weak. On the other hand, there are some differences in the Soret-bands region, which are caused by the exciton coupling between the **Z*n*** and the 5,15-bisphenylethylated Zn(II) porphyrin part owing to the large transition moments of the Soret bands ($S_0 \rightarrow S_2$).[14b] It is interesting to note that a selective photoexcitation of the *meso*−*meso* linked porphyrin arrays is possible at 550−560 nm.

The steady-state fluorescence spectra of **Z1A**−**Z24A** are shown in the insets of Figure 2, along with those of 1:1 mixtures of acceptor-free *meso*−*meso* linked porphyrin arrays (**Z1**, **Z2**, **Z3**, **Z6**, **Z12**, and **Z24**) and the porphyrin **4**. Upon photoexcitation at 550−560 nm corresponding to a selective excitation at the *meso*−*meso* linked porphyrin array, 1:1 mixtures of *meso*−*meso* linked Zn(II) porphyrin arrays and **4** exhibit the fluorescence predominantly from the *meso*−*meso* linked Zn(II) porphyrin arrays. The models **Z1A**−**Z12A** exhibit the fluorescence predominantly coming from the bisphenylethynylated Zn(II) porphyrin moiety, indicating the efficient, nearly quantitative EET processes. The fluorescence of **Z24A** comes largely from the acceptor moiety but also partly from the long donor porphyrin array (Supporting Information II). Here, it is noted that the donor emissions are completely overlapping the Q-band of the energy-accepting unit, being favorable for the rapid EET.

Figure 3a shows the comparison of the absorption spectra of **Z1A**−**Z24A** at the same concentration (9×10^{-8} M). At this dilute concentration, there is no serious aggregation, since the absorbance reflects the number of the porphyrins in the molecule. It is evident that the extensive exciton coupling within the *meso*−*meso* linked porphyrin array gives rise to a larger cross-section between 350 and 650 nm. This spectral feature is favorable for the light harvesting antenna function. Figure 3b compares the steady-state fluorescence taken for the excitation at 508 nm, where the **Z1A** model has practically no absorbance and **Z12A** and **Z24A** have the large absorbance due to the exciton coupling. In **Z2A**−**Z12A**, the incident light at this wavelength (508 nm) is efficiently delivered to the end energy acceptor, since the resultant fluorescence intensification is parallel to the increase in the absorbance at 508 nm. But the fluorescence intensity of **Z24A** is somewhat less than a value

(13) (a) Lin, V. S.-Y.; DiMagno, S. G.; Therien, M. J. *Science*, **1994**, *264*, 1105. (b) Arnold, D. P.; Nitschinsk, L. *Tetrahedron Lett*. **1993**, *34*, 693. (c) Anderson, H. L. *Inorg. Chem*. **1994**, *33*, 972.
(14) (a) Nakano, A.; Shimidzu, H.; Osuka, A. *Tetrahedron Lett*. **1998**, 39, 9489. (b) Nakano, A.; Yasuda, Y.; Yamazaki, T.; Akimoto, S.; Yamazaki, I.; Miyasaka, H.; Itaya, A.; Murakami, M.; Osuka, A. *J. Phys. Chem. A* **2001**, *105*, 4822.
(15) Lindsey, J. S.; Schreiman, I. C.; Hsu, H. C.; Kearney, P. C.; Marguerettaz, A. M. *J. Org. Chem.* **1987**, *52*, 827.
(16) DiMagno, S. G.; Lin, V. S.-Y.; Therien, M. J. *J. Org. Chem*. **1993**, *58*, 5983.
(17) (a) Sonogashira, K.; Tohda, Y.; Hagihara, N. *Tetrahedron Lett.* **1975**, 4467. (b) Lindey, J. S.; Prathapan, S.; Johnson, T. E.; Wagner, R. W. *Tetrahedron* **1994**, *50*, 8941.
(18) (a) Zhou, X.; Chan, K. S. *J. Org. Chem*. **1998**, *63*, 99. (b) Shultz, D. A.; Lee, H.; Kumar, R. K.; Gwaltney, K. P. *J. Org. Chem*. **1999**, *64*, 9124. (c) Mizutani, T.; Wada, K.; Kitagawa, S. *J. Am. Chem. Soc*. **2001**, *123*, 6459. (d) Deng, Y.; Chang, C. K.; Nocera, D. G. *Angew. Chem., Int. Ed*. **2000**, *39*, 1066. (e) Aratani, N.; Osuka, A. *Org. Lett*. **2001**, *3*, 4213. (f) Yu, L.; Lindsey, J. S. *Tetrahedron* **2001**, *57*, 9285. (g) Hyslop, A. G.; Kellett, M. A.; Iovine, P. M.; Therien, M. J. *J. Am. Chem. Soc*. **1998**, *120*, 12676.

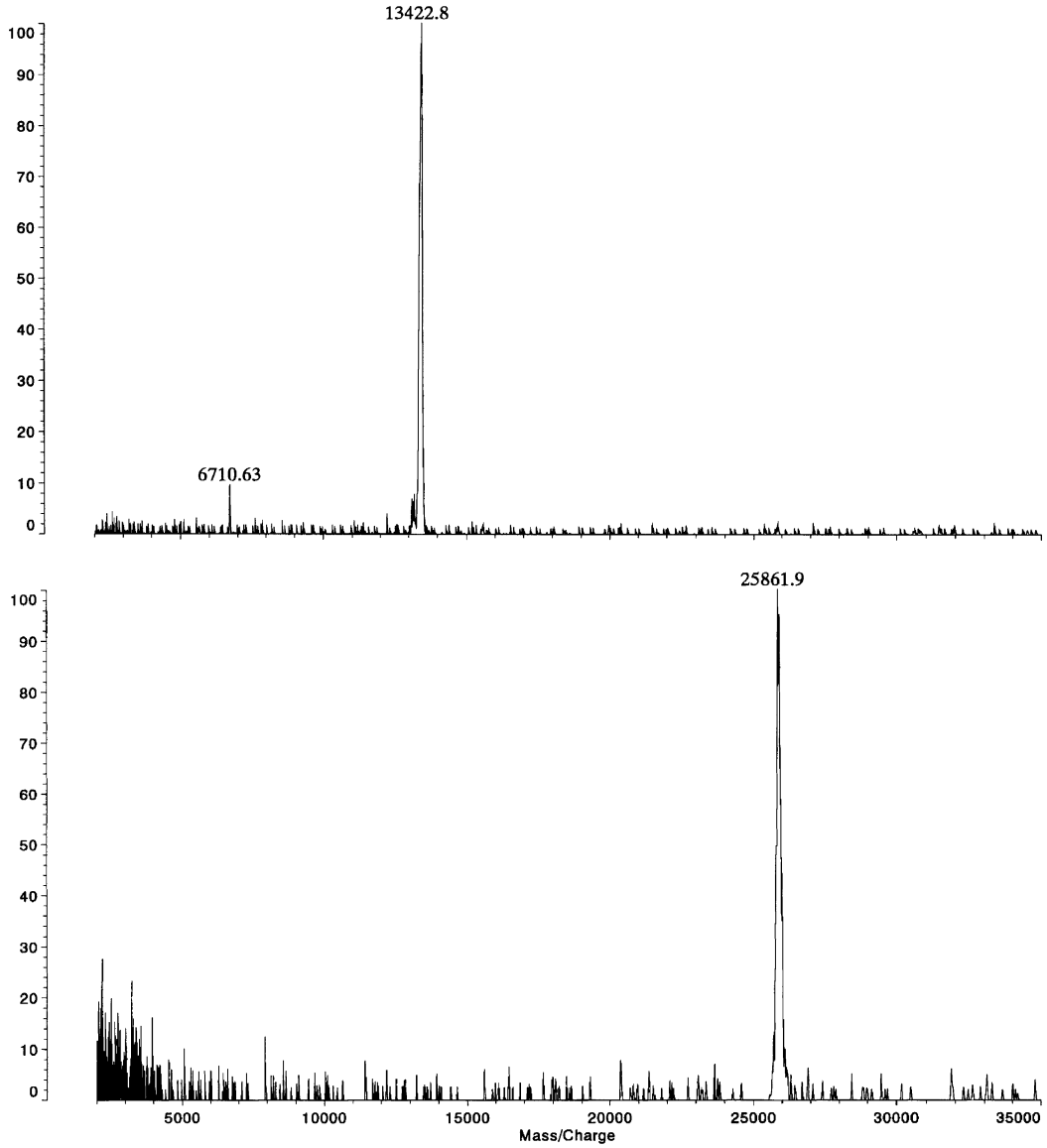

Figure 1. MALDI-TOF mass spectra of **Z12A** (upper) and **Z24A** (lower) recorded in positive ion mode with 9-nitroanthracence as matrix.

expected from its absorbance, indicating that the intramolecular EET is also efficient but not quantitative.

Transient Absorption Spectra.The transient absorption spectra of **Z1A**, **Z2A**, **Z3A**, **Z6A**, **Z12A**, and **Z24A** were taken by the selective S_1-excitation of the *meso*−*meso* linked porphyrin arrays at the Q-bands (Figure 4). The transient absorption spectrum of **Z1A** at a 2-ps delay time indicated a bleaching around 420 nm due to the depletion of the *meso*−*meso* linked porphyrin array (energy donor), which decayed quickly with $\tau = 1.6$ ps (Figure 5a). Along this spectral change, a new bleaching at 650 nm due to the depletion of the bisphenylethynylated Zn(II) porphyrin (energy acceptor) was observed to be growing with $\tau = 2.5$ ps (Figures 4a and 5a). Therefore, these two spectral changes indicate the efficient intramolecular EET from the *meso*−*meso* linked porphyrin array to the bisphenylethynylated Zn(II) porphyrin. Essentially the similar transient absorption spectra and temporal profiles were observed for **Z2A**, **Z3A**, **Z6A**, **Z12A**, and **Z24A** (Figures 4 and 5). On the basis of these data, the EET rate constants have been determined for **Z2A**, $(3.3\ \text{ps})^{-1}$; **Z3A**, $(5.5\ \text{ps})^{-1}$; **Z6A**, $(21\ \text{ps})^{-1}$; **Z12A**, $(63\ \text{ps})^{-1}$; and **Z24A**, $(108\ \text{ps})^{-1}$.

Transient Absorption Anisotoropy Decay Analysis. We have also carried out the femtosecond transient absorption anisotropy decay measurements for **Z1A**, **Z2A**, **Z3A**, and **Z6A** (Figure 6). The transition dipole of the S_1-state of the *meso*−*meso* linked porphyrin-array donor has been shown to align along the long molecular axis,[10c] and that of the lowest S_1-state of the 5,15-bisphenylethynyl Zn (II) porphyrin acceptor has been considered to align along the 5,15-direction.[13a] Therefore, in **Z2A**, **Z3A**, and **Z6A**, the key transition dipole moments of the donor and acceptor are placed in an orthogonal arrangement in their lowest excited states. Accordingly, a large anisotropy change is expected during the energy transfer processes.[10c] The anisotropy dynamics of **Z1A** probed at 480 nm exhibit only a rapid decay with $\tau = 0.2$ ps. In the case of **Z2A**, at 470 nm probe wavelength, we observed an initial rapid anisotropy decay with $\tau = 0.2$ ps, followed by an anisotropy rise with $\tau = 3.3$ ps (Figure 6b). The time constant of the anisotropy rise matches nicely with the EET rate constant. We observed similar behaviors for both **Z3A** and **Z6A**, a rapid anisotropy decay with $\tau = 0.2$ ps followed by an anisotropy rise with $\tau = 5.5$ ps in **Z3A** and a rapid anisotropy decay with $\tau = 0.2$ ps followed by

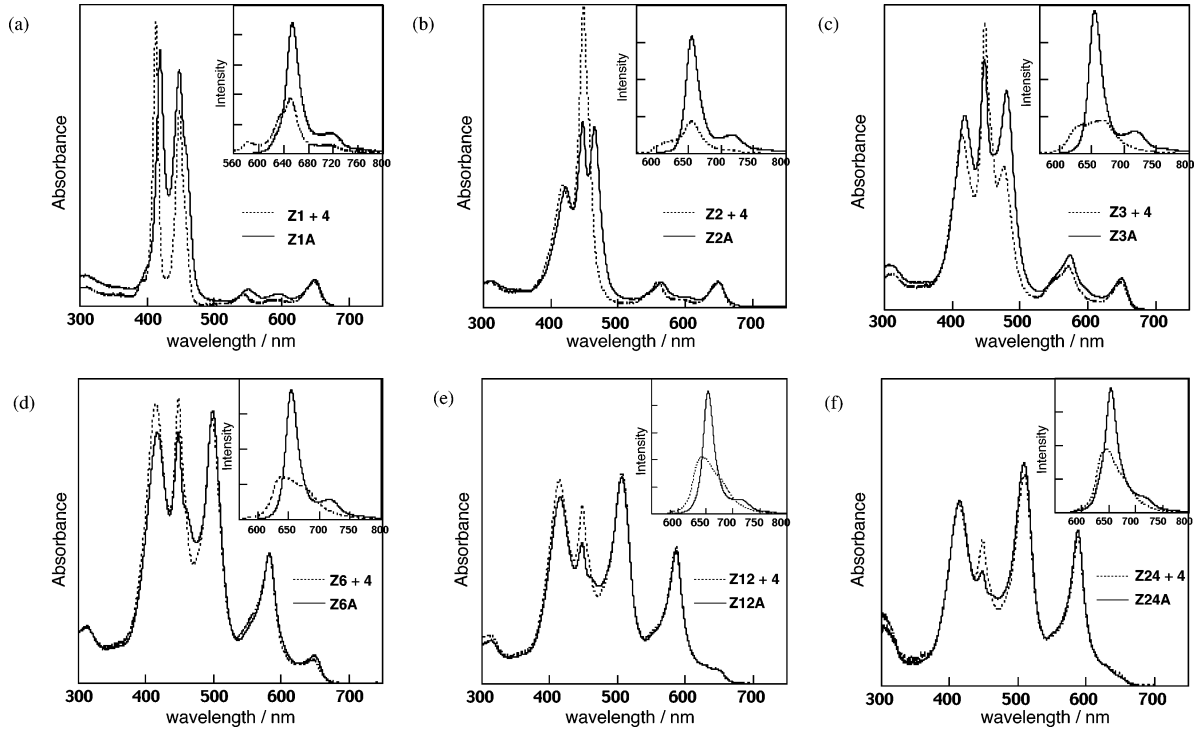

Figure 2. Absorption and fluorescence spectra of (a) **Z1A**, (b) **Z2A**, (c) **Z3A**, (d) **Z6A**, (e) **Z12A**, and (f) **Z24A**. Fluorescence spectra (shown in insets) were taken for excitation at their Q-bands. Solid lines are for **Zn**A, and broken lines are for 1:1 mixtures of **Zn** and **4**.

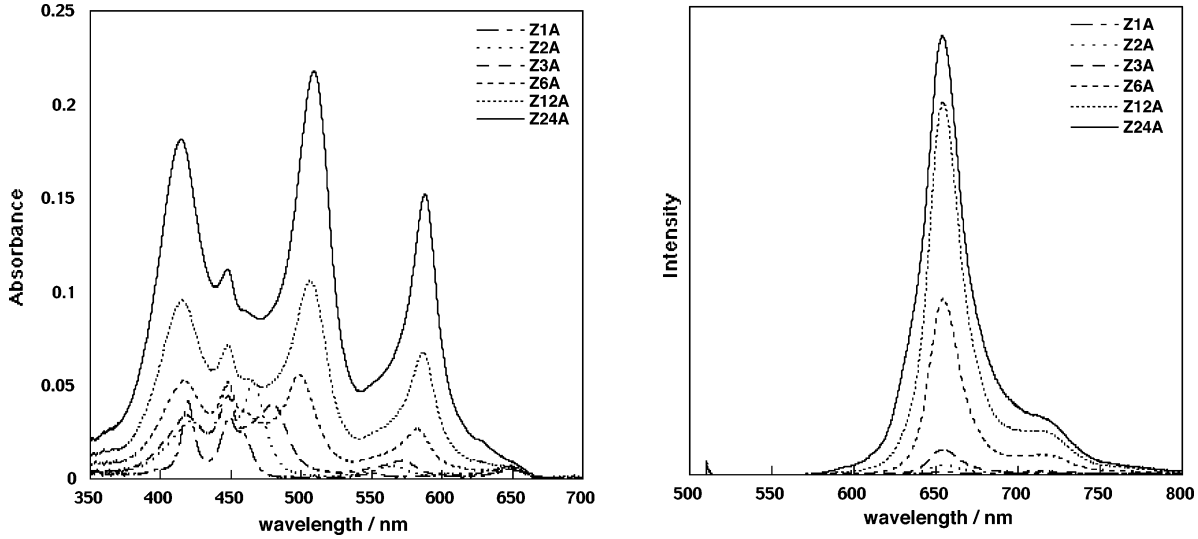

Figure 3. (a) Absorption and (b) fluorescence spectra of **Z1A**−**Z24A** at 9×10^{-8} M in THF. Fluorescence spectra were taken for excitation at 508 nm.

an anisotropy rise with $\tau = 21$ ps in **Z6A**, respectively (Figure 6c and d). The fast anisotropy decay with $\tau = 0.2$ ps indicates a coherent coupling time, while the observed anisotropy rise with slower time constants can be ascribed to the intramolecular energy transfer.

Discussion

The intramolecular EET events in **Z1A**−**Z24A** have been confirmed by the steady-state fluorescence and transient absorption measurements. The exciton coupling within the *meso*−*meso* linked Zn(II) porphyrin arrays causes the alteration and extension of the absorption spectral shapes, which are quite favorable for the light harvesting antenna function. Captured light energy is then delivered efficiently to the energy-accepting site in all the models **Z1A**−**Z24A**. The EET is almost quantitative in **Z1A**, **Z2A**, **Z3A**, **Z6A**, and **Z12A** but is not quantitative in **Z24A** as judged from Figure 3. The large electronic interaction between the directly *meso*−*meso* linked neighboring porphyrins must be responsible for the EET.

The anisotropy decay measurements have indicated that the present EET processes are accompanied by a large change in the direction of the transition dipole moment. In the case of **Z1A**, the anisotropy decay dynamics become complicated mainly due to the fact that a broad absorption band around 450 nm is not solely due to the acceptor Soret band but a mixture with the exciton split Soret band arising from excitonic interactions between donor and acceptor. Thus, even in the magic angle detection at 460 nm upon photoexcitation of **Z1A** at 400 nm, we observed rise and decay components due to the simultaneous participation of donor and acceptor bleaching

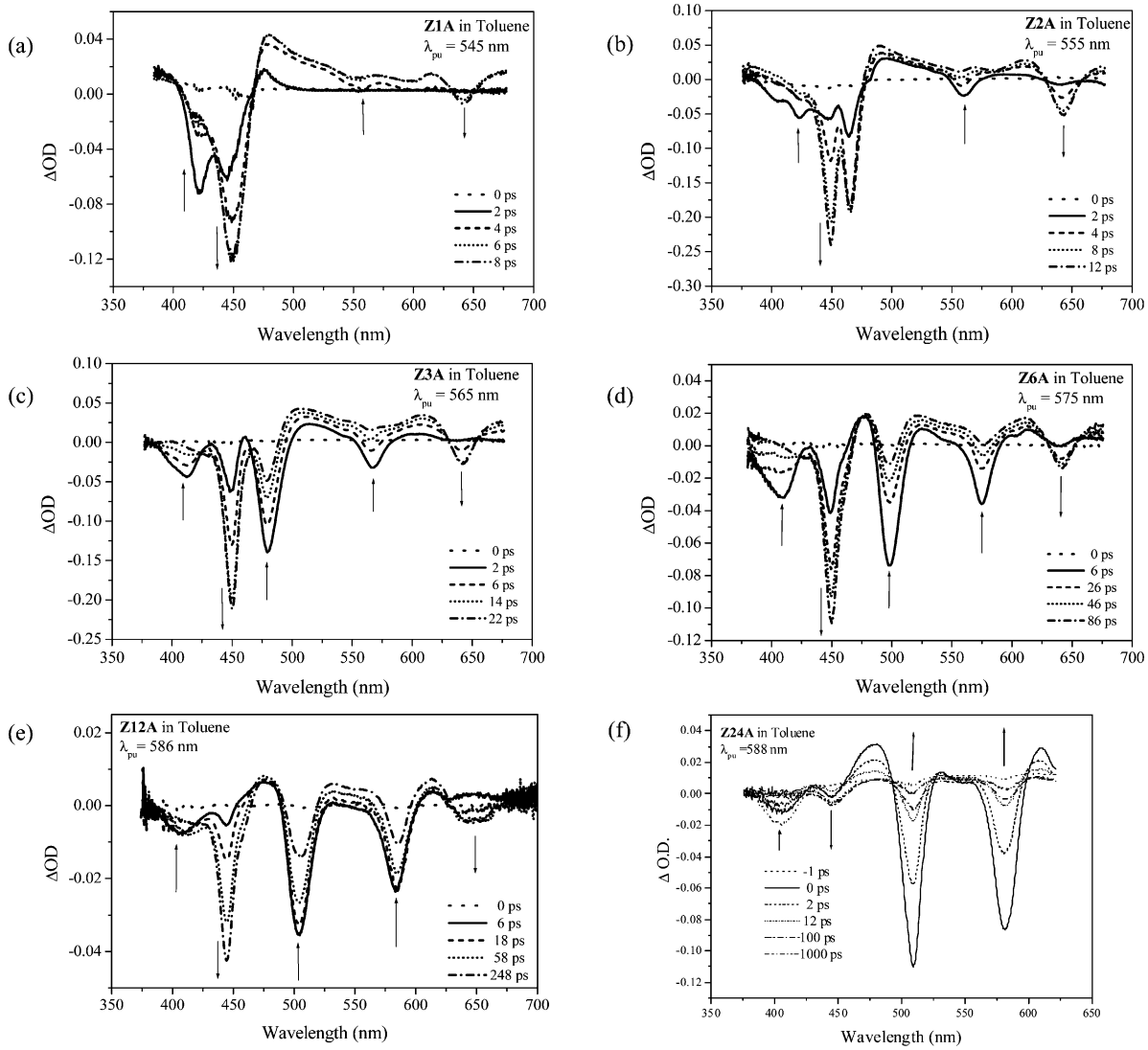

Figure 4. Transient absorption and fluorescence spectra of (a) **Z1A**, (b) **Z2A**, (c) **Z3A**, (d) **Z6A**, (e) **Z12A**, and (f) **Z24A**.

recoveries in the energy transfer process (Supporting Information III). In the case of **Z2A**, we observed similar phenomena especially at 470 nm probe wavelength, which contains a contribution from the exciton split Soret band between donor and acceptor. This process should be sensitive to the probe wavelength because the exciton split Soret band and the Soret band of the acceptor are overlapped at around 450 nm in the case of **Z1A**. At 480 nm probe, the contribution from the exciton split Soret band becomes reduced. The anisotropy dynamics of **Z1A**, probed at 480 nm, contains the initial rise due to the fast equilibrium between B_x and B_y polarizations of the donor part followed by a relatively slow energy transfer process with $\tau = \sim 2$ ps. The initial anisotropy decay of **Z6A** has also been assigned to the fast equilibrium between B_x and B_y polarizations, which reflects the coherent coupling time in preparing a large dipole (coherently coupled one) along the long axis of the array, while a slow anisotropy rise with $\tau = \sim 21$ ps can be assigned to the EET, because the time constant agrees with the EET rate constant $(21\ \text{ps})^{-1}$ and the donor and acceptor dipole moments are arranged orthogonal to each other. We observed similar behaviors in **Z2A** and **Z3A**.

In the next step, we consider the dependence of the EET rate constant upon the number of the porphyrins in the array. First, let us consider that excited states on the porphyrin array are excitons, and their quantum-mechanical wave functions extend coherently over the entire array. Such exciton states are formed due to ample inter-porphyrin interactions which, as the first approximation, can be regarded as brought about by the electrostatic interaction between transition dipoles at neighboring porphyrins in the array. Participating in the interaction at each porphyrin is a component with a transition dipole parallel to the array axis in the doubly degenerate S_1 transitions. When the array is composed of N porphyrins, the lowest exciton state on the array can be represented by

$$|d\rangle = \sqrt{\frac{2}{N+1}}\sum_{n=1}^{N}\sin\left(\frac{\pi}{N+1}n\right)|n\rangle \qquad (1)$$

where $|n\rangle$ represents a state of the array that the nth porphyrin therein is excited with a transition dipole parallel to the array while all the other porphyrins are unexcited. The energy eigenvalue of $|d\rangle$ is given by

$$E_d = E_0 + 2\Delta\cos[\pi/(N+1)] \qquad (2)$$

where E_0 represents the excitation energy of the S_1 transition

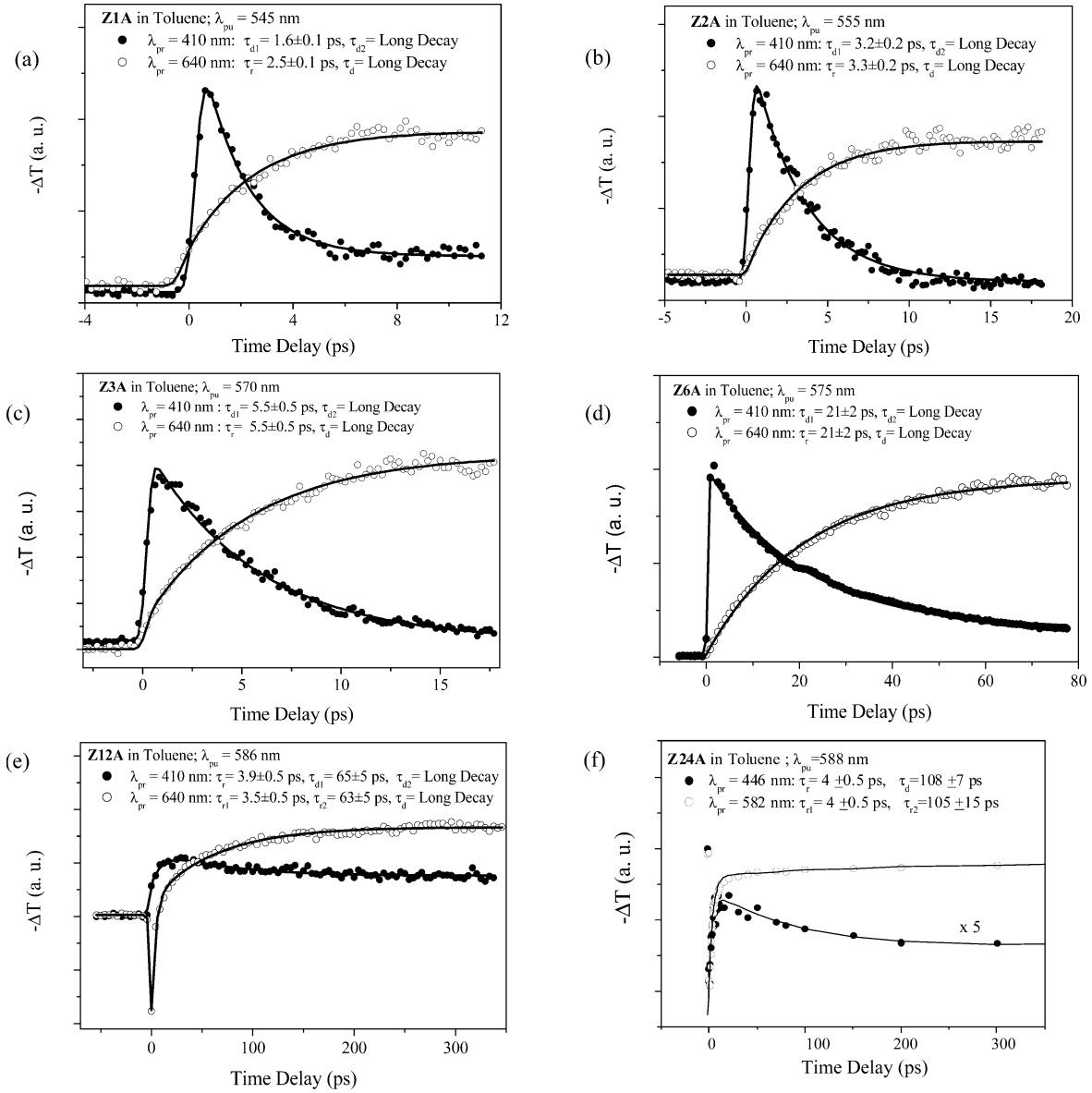

Figure 5. Temporal time profiles of the transient absorption spectra of (a) **Z1A**, (b) **Z2A**, (c) **Z3A**, (d) **Z6A**, (e) **Z12A**, and (f) **Z24A**.

of a single porphyrin, and Δ represents the excitonic interaction between neighboring porphyrins in the array. The total transition dipole of this donor state $|d\rangle$ is parallel to the array axis with a magnitude

$$\sqrt{\frac{2}{N+1}}\sum_{n=1}^{N}\sin\left(\frac{\pi}{N+1}n\right)\mu = \sqrt{\frac{2}{N+1}}\cot\left(\frac{\pi}{2N+2}\right)\mu \quad (3)$$

where μ represents the magnitude of the S_1 transition dipole of a single porphyrin.

Next, we consider the acceptor state of the EET at the 5,-15-bisphenylethynyl porphyrin. The attachment of phenylacethylene moieties at the 5 and 15 positions breaks the 2-fold degeneracy of the S_1 transitions at the acceptor porphyrin in such a way that the component with a transition dipole parallel to the 5,15 direction becomes the lowest excited state.[13a] EET from the donor takes place with energies of its fluorescence spectrum as long as it overlaps the absorption spectrum of the acceptor. In the present case, the fluorescence spectrum of the porphyrin-array donor covers completely the absorption spectrum of the acceptor porphyrin in the energy region of its S_1 transitions, as mentioned earlier. In this situation, it seems reasonable to consider that the acceptor state for the EET is a mixture of the S_1 component with the 5,15-transition dipole and the other component with the perpendicular 10,20-transition dipole. The 5,15-transition dipole is perpendicular to the long molecular axis of the porphyrin-array donor, while the 10,20-transition dipole is parallel to it. Since all the porphyrins in the array have a transition dipole parallel to the array axis in the donor state for the EET, they do not interact with the former at the acceptor porphyrin at least in the transition-dipole approximation. Therefore, we consider that the observed rapid EET from the donor to the acceptor takes place via the S_1 component with the 10,20-transition dipole at the acceptor porphyrin.

The traditional theory on the EET rate constant is Förster's one,[19] which considers that EET arises by the electrostatic interaction between transition dipoles at the donor and the

(19) (a) Förster, T. *Ann. Phys.* **1948**, *2*, 55. (b) Förster, T. *Discuss. Faraday Soc.* **1959**, *27*, 7.

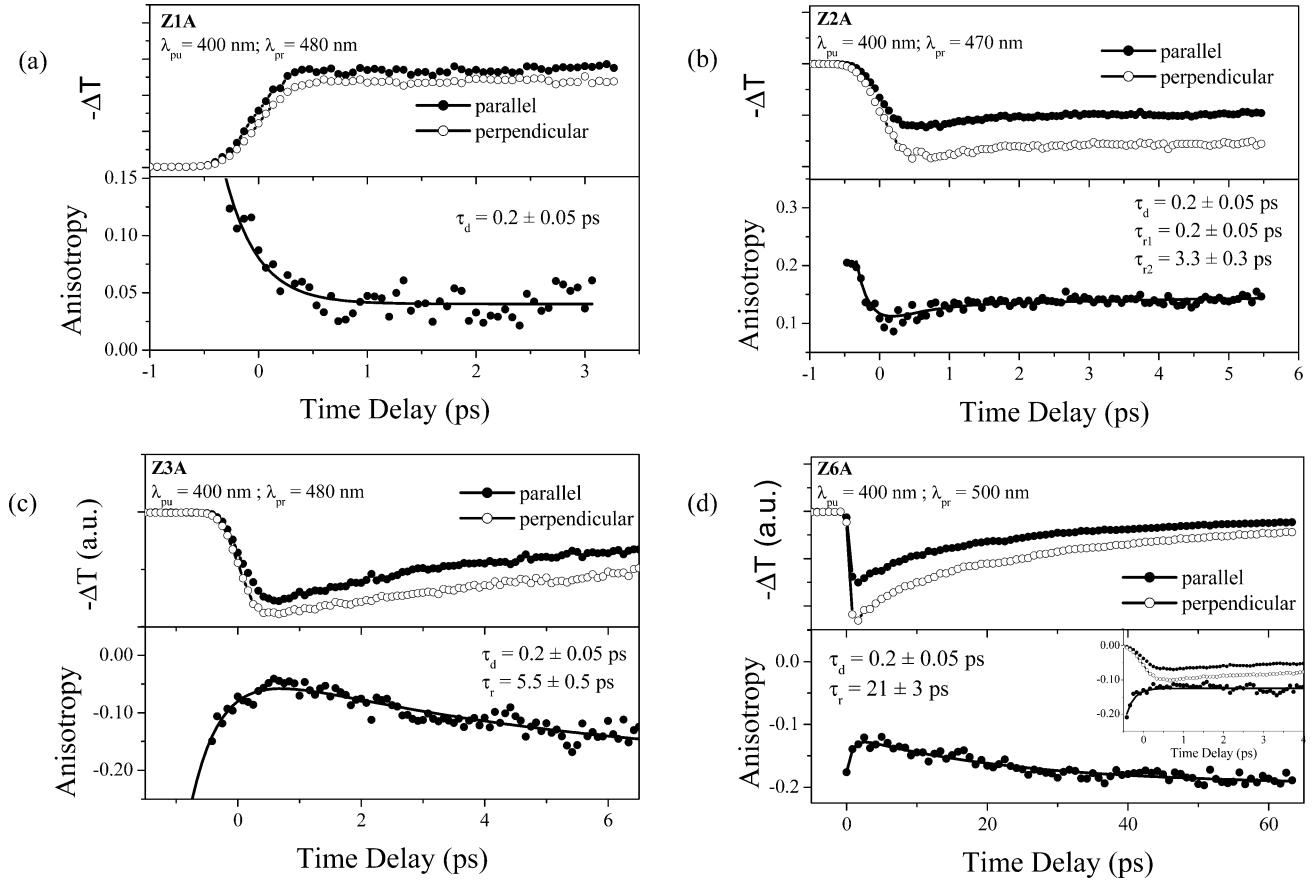

Figure 6. Femtosecond transient absorption anisotropy decays of (a) **Z1A**, (b) **Z2A**, (c) **Z3A**, and (d) **Z6A**.

acceptor. In the present problem, the donor is regarded as the tightly bound entire porphyrin array with a single total transition dipole of eq 3 parallel to the array axis and located at the center of the array. Its EET interaction with the 10,20-transition dipole on the acceptor porphyrin is given by $[2/(N+1)]^{1/2}\cot[\pi/(2N+2)](R_1/R)^3J$, where R represents the distance from the acceptor porphyrin to the center of the porphyrin array and R_1 and J represent, respectively, the distance and the EET coupling in **Z1A** for $N = 1$. Förster's formula is given by the lowest (i.e., second-order) perturbation in the EET interaction, that is, by Fermi's Golden Rule.[8c] The rate constant for the EET obtained is given by

$$k_N = \frac{4\pi J^2}{\hbar(N+1)}\left(\frac{R_1}{R}\right)^6 \cot^2\left(\frac{\pi}{2N+2}\right)\int I_a(E)L_N(E)\,dE \quad (4)$$

where $I_a(E)$ and $L_N(E)$ represent respectively the absorption spectrum of the acceptor porphyrin and the fluorescence spectrum of the array of N porphyrins as the donor, both being normalized as

$$\int I_a(E)\,dE = \int L_N(E)\,dE = 1 \quad (5)$$

In eq 4, it has been assumed that the absorption spectrum of the S_1 component with the 5,15-transition dipole and that of the other component with the perpendicular 10,20-transition dipole on the acceptor porphyrin can be regarded as similar to each other in the energy range covered by the fluorescence spectrum of the porphyrin-array donor, both being approximated as proportional to $I_a(E)$.

The value of J is concerned with the actual degree of mixture of the S_1 component with the 10,20-transition dipole in the acceptor state. Instead of actually calculating the degree of the mixture, let us be content with estimating J as an effective EET coupling from the observed value of k_1, since J is practically more useful. For $N = 1$, eq 4 reduces to

$$k_1 = \frac{2\pi}{\hbar}J^2\int I_a(E)L_1(E)\,dE \quad (6)$$

We observed $k_1 = (\sim 2.5\text{ ps})^{-1}$, and also $\int I_a(E)L_1(E)\,dE$, called Förster's overlap integral, to be $(\sim 2500\text{ cm}^{-1})^{-1}$. These values enable us to derive $J \approx 29\text{ cm}^{-1}$ from eq 6.

Dependence of the EET rate constant on the number (N) of porphyrins in the donor-array manifests itself most purified in the ratio of k_N/k_1, which is given by

$$\frac{k_N}{k_1} = \frac{2}{N+1}\left(\frac{R_1}{R}\right)^6 \cot^2\left(\frac{\pi}{2N+2}\right)\frac{\int I_a(E)L_N(E)\,dE}{\int I_a(E)L_1(E)\,dE} \quad (7)$$

In k_N of eq 4, both the effective EET coupling J in **Z1A** and Förster's overlap integral have some ambiguities arising from the approximation for $I_a(E)$ mentioned below eq 5. The ratio of k_N/k_1 does not include J, and also the ratio of Förster's overlap integrals at the right-hand end of eq 7 is nearly independent of N with a magnitude of about 1.0 except for $N = 3$ where it is about 0.87. Therefore, the N dependence of k_N/k_1 can be used as a check of theories for EET.

Table 1. Observed and Calculated EET Rate Constants

model	R^a (Å)	$k_{obs}^{-1\,b}$ (ps)	$k_N^{-1\,c}$ (ps)	$k_N^{-1\,d}$ (ps)	$k_N^{-1\,e}$ (ps)
Z1A	12.7	2.5 ± 0.1			
Z2A	16.9	3.3 ± 0.2	6.9	5.0	3.4
Z3A	21.0	5.5 ± 0.5	20	7.5	5.9
Z6A	33.6	21 ± 2	160	15	23
Z12A	58.6	63 ± 5	2300	30	70
Z24A	109	108 ± 7	49 000	60	163

[a] Center-to-center distances between the donor and the acceptor. [b] EET rate constants measured by the transient absorption spectra. [c] EET rate constants calculated by eq 7. [d] EET rate constants calculated by eq 8. [e] EET rate constants calculated by eqs 13 and 14 for $L = 4$.

The center-to-center distance R between the donor and the acceptor was estimated by the CPK models, being listed in Table 1. For $k_1 = (\sim 2.5\ \text{ps})^{-1}$, this eq 7 gives $k_2 = (\sim 6.9\ \text{ps})^{-1}$, $k_3 = (\sim 20\ \text{ps})^{-1}$, $k_6 = (\sim 160\ \text{ps})^{-1}$, $k_{12} = (\sim 2.3\ \text{ns})^{-1}$, and $k_{24} = (\sim 49\ \text{ns})^{-1}$. These values are too small in comparison with the observed ones, as shown also in Table 1. We see thus that the observed data cannot be described by Förster's theory. The rate constant with the R^{-6} dependence therein decreases too rapidly with R to reproduce the observed data.

Origins of inapplicability of Förster's theory mentioned above can be found in its two assumptions that excited states on the porphyrin array are excitons which extend coherently over the entire array and that the entire array can be regarded as a single suprachromophore with a single transition dipole in the calculation of the EET rate constant. Concerning the first assumption, it is very difficult to consider that the coherence length of an exciton extends over the entire array for long models **Z12A** and **Z24A**. As a limit for breaking the first assumption, let us consider that excited states on the porphyrin array have no coherence among porphyrins. In this limit, an excitation is localized at a single porphyrin in the array, and it carries correctly a single transition dipole. Considering further the weak-coupling limit in the EET, excitations on the porphyrin array are regarded as maintained in thermal equilibrium in the course of EET from the donor to the acceptor. Since each porphyrin in the array has the same excitation energy, an excitation can be found at each porphyrin with the same probability given by $1/N$ in thermal equilibrium. An excitation found at the $n = 1$ porphyrin can be transferred to the acceptor porphyrin with a probability k_1 given by eq 6, and that found at the $n = 2$ porphyrin can be transferred with a probability of $k_1(R_1/R_2)^6$ where R_2 represents the center-to-center distance between the $n = 2$ porphyrin in the array and the acceptor porphyrin. Since $(R_1/R_2)^6 = \sim 0.049$, we can neglect EET from an excitation found at the $n = 2$ porphyrin and also from that found at remoter porphyrins for $n \geq 3$. Therefore, the rate constant for EET to the acceptor porphyrin from the donor array composed of N porphyrins is given by

$$k_N = k_1/N \tag{8}$$

For $k_1 = (\sim 2.5\ \text{ps})^{-1}$, this eq 8 gives $k_2 = (\sim 5.0\ \text{ps})^{-1}$, $k_3 = (\sim 7.5\ \text{ps})^{-1}$, $k_6 = (\sim 15\ \text{ps})^{-1}$, $k_{12} = (\sim 30\ \text{ps})^{-1}$, and $k_{24} = (\sim 60\ \text{ps})^{-1}$. These values are not very bad but differ considerably from the observed EET rate constants (Table 1).

Let us check the second assumption in Förster's formula that the entire porphyrin array can be regarded as a single suprachromophore with a single transition dipole in the calculation of the EET rate constant. In reality, individual porphyrins coupled coherently with each other in the donor state of eq 1 carry well-defined transition dipoles whose vectorial sum gives the total transition dipole of eq 3 appearing in Förster's formula of eq 4. These individual transition dipoles $[2/(N+1)]^{1/2} \sin[\pi n/(N+1)]\mu$ for $n = 1, 2, \cdots, N$ at each porphyrin in the donor array interact with the transition dipole at the acceptor porphyrin with different strengths because of differences in the interaction distance. Interaction of the nth porphyrin in the array is given by $[2/(N+1)]^{1/2} \sin[\pi n/(N+1)](R_1/R_n)^3 J$, where R_n represents the center-to-center distance between the nth prophyrin in the array and the acceptor porphyrin and J represents the effective EET coupling between the $n = 1$ porphyrin in the array and the acceptor porphyrin in eq 6. Taking into account the interaction of these transition dipoles with the acceptor transition dipole, we get the correct total interaction strength for EET between the porphyrin-array donor and the acceptor porphyrin, as

$$V_N = J\sqrt{\frac{2}{N+1}}\sum_{n=1}^{N}\sin\left(\frac{\pi}{N+1}n\right)\left(\frac{R_1}{R_n}\right)^3 \tag{9}$$

Since $(R_1/R_2)^3 = \sim 0.22$ and $(R_1/R_3)^3 = \sim 0.081$, terms at least for $n = 2$ and 3 in the summation on the right-hand side cannot be neglected in comparison with the term for $n = 1$. On the basis of Fermi's Golden Rule,[8c] the rate constant for the EET caused by V_N of eq 9 is given by

$$k_N = \frac{2\pi}{\hbar}V_N^2\int I_a(E)L_N(E)\,dE \tag{10}$$

It must be taken into account also here that the coherence length of an exciton in the donor array is not so long as the entire array at least for **Z12A** and **Z24A**, because of decoherence disturbances increasing in number with the array length. Therefore, let us consider that the lowest exciton state on the array can cover coherently at most L porphyrins. Accordingly, it is only when $N \leq L$ that we can use eq 10 with eq 9 for describing the rate constant of the EET. When $N > L$, an exciton with the coherence length L can be found at $N - L + 1$ locations on the array composed of N porphyrins, with the same energy given by eq 2 for $N = L$ therein. Considering the weak-coupling limit in the EET, excitations on the porphyrin array are regarded as maintained in thermal equilibrium in the course of EET from the donor to the acceptor. In thermal equilibrium, each exciton state can be realized with the same probability given by $1/(N - L + 1)$. An exciton found at the location nearest to the acceptor porphyrin transfers its excitation energy to the acceptor with a probability of k_L given by eq 10 for $N = L$ therein. An exciton found at the location next nearest to the acceptor porphyrin transfers its excitation energy with a probability of k_L' given by eq 10 with V_N therein changed into

$$V_L' = J\sqrt{\frac{2}{N+1}}\sum_{n=1}^{L}\sin\left(\frac{\pi}{N+1}n\right)\left(\frac{R_1}{R_{n+1}}\right)^3 \tag{11}$$

instead of V_L for k_L. Since k_L' has only a magnitude on the order of $(R_1/R_2)^6$ ($=\sim 0.049$) times as small as k_L, we can neglect EET from an exciton found at the next-nearest location and also excitons found at remoter locations even if they exist. Therefore,

we obtain the rate constant for EET to the acceptor porphyrin from the array composed of N porphyrins as

$$k_N = k_L/(N - L + 1), \text{ for } N > L \tag{12}$$

As mentioned earlier, the N dependence of the ratio k_N/k_1 can be used as a check of theories for EET. It is given by

$$\frac{k_N}{k_1} = \frac{2}{N+1}\left[\sum_{n=1}^{N} \sin\left(\frac{\pi}{N+1}n\right)\left(\frac{R_1}{R_n}\right)^3\right]^2 \frac{\int I_a(E)L_N(E)\,dE}{\int I_a(E)L_1(E)\,dE}, \text{ for } N \le L \tag{13}$$

and

$$k_N/k_1 = (k_L/k_1)/(N - L + 1), \text{ for } N > L. \tag{14}$$

We note here that eq 8 is a special case of eq 14 for $L = 1$.

The coherent length L has been estimated to be about 4 on the present porphyrin array.[20,21] When $L = 4$ and $k_1 = (\sim 2.5\ \text{ps})^{-1}$, eqs 13 and 14 give $k_2 = (\sim 3.4\ \text{ps})^{-1}$, $k_3 = (\sim 5.9\ \text{ps})^{-1}$, $k_6 = (\sim 23\ \text{ps})^{-1}$, $k_{12} = (\sim 70\ \text{ps})^{-1}$, and $k_{24} = (\sim 163\ \text{ps})^{-1}$. These values are in good agreement with the observed ones except the longest model **Z24A** (Table 1). Therefore, this approach seems most suitable in reproducing the observed rate constants of EET from the porphyrin array to the acceptor porphyrin.

The deviation of k_{24} from the observed value may be due to a breakdown of the assumption that an exciton with a coherence length L (~ 4) can be found with the same probability at any site in the entire porphyrin-array donor in thermal equilibrium even when it has a number of porphyrins as many as 24. In such a long donor array, a little slanting in the porphyrin-site energy causes a substantial deviation from the assumed equal distribution of exciton location. In the present case, donor porphyrins near to the acceptor porphyrin could have site energies lower than remoter porphyrins due to influence from the acceptor porphyrins, and an exciton could be found more on the former than on the latter in thermal equilibrium in a long array. Such an unequal distribution in exciton location will give a k_{24} larger than that given in Table 1. Increased conformational heterogeneity in such a long array might be another cause for this deviation. Such an effect may be also responsible for the incomplete EET in **Z24A.**

If the center-to-center distance R_1 between the $n = 1$ porphyrin in the donor array and the acceptor porphyrin was much larger than the total length ΔR of the donor array composed of N porphyrins, differences among R_n's could be neglected on the right-hand side of eq 9. Accordingly, all the R_n's could be approximated by the distance R between the acceptor porphyrin and the center of the porphyrin-array donor. Thereby, eq 10 would reduce to eq 4 that can be obtained by Förster's formula. In reality, however, R_1 ($= \sim 12.7$ Å) is not much larger than ΔR ($= \sim 8.3$ Å) even for $N = 2$, and eq 10 gives the k_N value much different from eq 4, the difference becoming enormous when N becomes larger. Such a difference can be regarded as a size effect of the donor and/or the acceptor for EET, where at least one of them is a molecular aggregate whose excited states are excitons and simultaneously the physical size of the aggregate is not much smaller than the average donor−acceptor distance. In this situation, Förster's formula is not correct in a sense that it deviates from the rate constant of EET derived correctly from the lowest (i.e., second-order) perturbational expansion in the EET coupling between the donor and the acceptor, although Förster's formula itself is also second order in the coupling. Such a formula that is correct in the weak-coupling limit has been presented by one of the present authors, Sumi.[8] It may be called a revised Förster formula. It has successfully been applied to EET in the antenna system of photosynthesis where the situation mentioned above can widely be found.[9] In fact, the rate constant of eq 10 with eq 9 for the present problem corresponds to a special case in the general formula for the rate constant of EET given in ref 8.

In the present models, the acceptor porphyrin is connected with the adjacent porphyrin (P1) through a 1,4-phenylene spacer with the center-to-center distance $R_1 = \sim 12.7$ Å. P1 is naturally the edge porphyrin in the donor array. Additional attachment of the second porphyrin (P2) to **Z1A** leads to **Z2A** that has a center-to-center donor−acceptor distance of $R_2 = \sim 21.0$ Å. In such situations, the EET interaction between two molecules might have to be calculated more appropriately than by the transition-dipole approximation. For example, it might be calculated by the so-called monopole approximation[22] with a correct account of the spatial extension of the wave functions in the excited states of the molecules or by taking into account also electron-exchange effects. In these cases, the $(R_1/R_n)^3$ dependence of the terms for $n \ge 2$ in the summation on the right-hand side of eq 9 might be a little revised. After such a revision, these terms for $n \ge 2$ should still retain magnitudes not negligible in comparison with the first term therein. This situation is essential in reproducing the N dependence of the observed EET rate constant by k_N of the revised Förster's formula eq 10 with eq 9. On the contrary, eq 8 obtained by completely neglecting the spatial coherence of the exciton state gives k_N considerably smaller than the observed ones, mainly because it has been approximated in eq 8 to be only the $n = 1$ porphyrin in the donor array that takes part in EET to the acceptor porphyrin.

Conclusion

A series of *meso*−*meso* linked Zn(II) porphyrin arrays bearing a 5,15-bisphenylethynylated Zn(II) porphyrin were prepared for

(20) Previously, the coherent length (L) in the S_1-state of a *meso*−*meso* linked Zn(II) porphyrin array has been estimated to be ~ 5 on the basis of the equation developed by Knoester (Bakalis, L. D.; Knoester, J. *J. Phys. Chem. B* **1999**, *103*, 6620); $L = \sqrt{3\pi^2|\Delta E_0|/\gamma} - 1$ by letting the coupling strength $|\Delta E_0| = 270\ \text{cm}^{-1}$ and $\gamma = 236\ \text{cm}^{-1}$. The coupling strength was estimated from the ratio of the absorption coefficients of Soret and Q-bands in monomer ($\sim 1/16$). In this estimation, we only considered the dipole−dipole interaction between porphyrin moieties and may neglect the coupling originated from the through-bond effect. In the present work, we obtained a coupling strength V of $\sim 570\ \text{cm}^{-1}$ by plotting the peak positions of Q-bands and fitting to the equation of $E_k = E_0 + 2V\cos(\pi/(N+1))$. Now, L has been estimated to be ~ 4 on the basis of the following equation (Kakitani, T.; Kimura, A. *J. Phys. Chem. A* **2002**, *106*, 2173); $L = 1.38 + 1.33V/\gamma$. This empirical formula seems to be more applicable in our porphyrin array system because this model is based on the one-dimensional linear array system.

(21) A detailed study on the energy relaxation dynamics of a *meso*,*meso*′-dibrominated Zn(II) porphyrin array also predicts $N_c = \sim 4$; Ha, J. H.; Cho, H. S.; Kim, D.; Aratani, N.; Osuka, A. Submitted for publication.

(22) (a) Chang, J. C. *J. Chem. Phys*. **1977**, *67*, 3901. (b) Warshel, A.; Parson, W. W. *J. Am. Chem. Soc*. **1987**, *109*, 6143. (c) Parson, W. W.; Warshel, A. *J. Am. Chem. Soc*. **1987**, *109*, 6152. (d) Nagae, H.; Kakitani, T.; Katoh, T.; Mimuro, M. *J. Chem. Phys*. **1993**, *98*, 8012. (e) Alden, R. G.; Johnson, E.; Nagarajan, V.; Parson, W. W.; Law, C. J.; Cogdell, R. G. *J. Phys. Chem. B*, **1997**, *101*, 4667. (f) Krueger, B. P.; Scholes, G. D.; Fleming, G. R. *J. Phys. Chem. B*, **1998**, *102*, 5378.

the examination of EET systems involving a strongly coupled array of donor or acceptor. In all the model compounds including **Z24A**, the efficient intramolecular EET processes have been proven by the steady-state fluorescence measurement as well as the time-resolved transient absorption spectroscopy and ultrafast anisotropy decay measurements. The EET is almost quantitative in **Z1A** to **Z12A** but is competitive in **Z24A**. Long-distance yet efficient EET processes are realized through the exciton states whose coherence is extended over several porphyrin pigments in the *meso*−*meso* linked Zn(II) porphyrin arrays, as such in the natural photosynthetic light harvesting systems such as chlorosomes, LH1, and LH2. This strategy is very useful for the design of efficient artificial EET systems in the future. For these EET systems involving an aggregate, Sumi's revised Förster formula has been demonstrated to be useful for the analysis. These results may encourage further application of *meso*−*meso* linked porphyrin arrays for even longer EET and directed EET from a well-defined donor to an acceptor over an extremely long distance, since such a long array is now available in a discrete form. Finally, advantages of strongly coupled arrays of chromophores in antenna function should be emphasized in terms of fast EET and large absorption cross-section unless forming an energy-wasting sink.

Experimental Section

General Procedure. All reagents and solvents were of the commercial reagent grade and were used without further purification except when noted. Dry toluene and DMF were obtained by distillation. ^{1}H NMR spectra were recorded on a JEOL ALPHA-500 spectrometer, and chemical shifts were reported as the delta scale in ppm relative to $CHCl_3$ ($\delta = 7.260$). The spectroscopic grade THF was used as solvent for the spectroscopic measurements. UV−visible absorption spectra were recorded on a Shimadzu UV-2400PC spectrometer. Steady-state fluorescence emission spectra were recorded on a Shimadzu RF-5300PC spectrometer. Mass spectra were recorded on a JEOL HX-110 spectrometer, using a positive-FAB ionization method with accelerating voltage 10 kV and a 3-nitrobenzyl alcohol matrix, and/or on a Shimadzu/KRATOS KOMPACT MALDI4 spectrometer, using a positive-MALDI-TOF method. Preparative separations were performed by silica gel flash column chromatography (Merck Kieselgel 60 H Art. 7736) and silica gel gravity column chromatography (Wakogel C-200). Recycling preparative GPC−HPLC was carried out on a JAI LC-908 model using a combination of preparative JAI-GEL-3H and 2.5H columns for **Z1A**−**Z6A**, JAI-GEL 4H, 3H, and 2.5H for **Z12A**, and JAI-GEL 4H, 3H, and 3H for **Z24A** (chloroform eluant; flow rate 3.8 mL min^{-1}).

The dual-beam femtosecond time-resolved transient absorption spectrometer consisted of a self-mode-locked femtosecond Ti:sapphire oscillator (Coherent, MIRA), a Ti:sapphire regenerative amplifier (Clark MXR, CPA-1000) pumped by a Q-switched Nd:YAG laser (Clark MXR, ORC-1000), a pulse stretcher/compressor, OPA (Light Conversion, TOPAS) system, and an optical detection system. A femtosecond Ti:sapphire oscillator pumped by a CW Nd:YVO_4 laser (Coherent, Verdi) produces a train of ~80 fs mode-locked pulses with an averaged power of 650 mW at 800 nm. The amplified output beam regenerated by chirped pulse amplification (CPA) had ca. 150 fs pulse width and an average power of ca. 1 W at 1 kHz repetition rate, which was divided into two parts by a 1:1 beam splitter. One was color-tuned for the pump beam by an optical parametric generation and amplification (OPG-OPA) technique. The resulting laser pulse had a temporal width of ~150 fs in the UV/Vis/IR range. The pump beam was focused to a 1 mm diameter spot, and the laser fluence was adjusted to avoid damage to the sample by using a variable neutral-density filter. The other was focused onto a flowing water cell to generate a white light continuum, which was again split into two parts. One part of the white light continuum was overlapped with the pump beam at the sample to probe the transient, while the other part of the beam was passed through the sample without overlapping the pump beam. The time delay between pump and probe beams was controlled by making the pump beam travel along a variable optical delay line. The white light continuum beams after the sample were sent to a 15 cm focal length spectrograph (Acton Research) through each optical fiber and then detected by a dual-channel 512 channel photodiode array (Princeton Instruments). The intensity of the white light continuum of each 512 channel photodiode array was processed to calculate the absorption difference spectrum at the desired time delay between pump and probe pulses. For the transient absorption anisotropy decay ($r(t)$) measurements, the probe white light continuum pulse was set to have vertical polarization by using a sheet polarizer. Then, the excitation pulse was changed to have parallel or perpendicular polarization by rotating a half wave plate centered at 400 nm with respect to the polarization of the probe pulse. Finally, the transient absorption anisotropy decay can be obtained by the following equation.

$$r(t) = \frac{\Delta A_{\parallel} - \Delta A_{\perp}}{\Delta A_{\parallel} + 2\Delta A_{\perp}} \tag{15}$$

5-[4-(4,4,5,5-Tetramethyl-1,3,2-dioxaborolan-2-yl)phenyl]-15-(3,5-dioctyloxyphenyl)porphyrin 1. 4-(4,4,5,5-Tetramethyl-1,3,2-dioxaborolan-2-yl)benzaldehyde was prepared from 4-formylphenylboronic acid and 2,3-dimethyl-2,3-butandiol (pinacol, 1.2 equiv) by using a Dean−Stark trap apparatus in 92% yield. A solution of 2,2′-dipyrrylmethane[23] (1.40 g, 9.50 mmol), 3,5-dioctyloxybenzaldehyde (1.74 g, 4.75 mmol), and the boronate-appended benzaldehyde (1.10 g, 4.75 mmol) in dry CH_2Cl_2 (1.5 L) was stirred under N_2 and shielded from light. Trifluoroacetic acid (TFA) (0.460 mL, 5.60 mmol) was added via syringe, and the solution was stirred for 3 h at room temperature. DDQ (3.78 g, 16.6 mmol) was added to the solution, and the resulting solution was stirred for an additional 3 h. After the reaction mixture was neutralized by triethylamine and passed over a short silica gel column to remove polymeric materials, the solvent was removed by a rotary evaporator and the residue was separated by silica gel column chromatography with CH_2Cl_2/*n*-hexane. The first fraction was 5,15-bis(3,5-dioctyloxyphenyl)porphyrin, and the second fraction was the desired porphyrin **2**. The product was recrystallized from CH_2Cl_2−MeOH. Yield; 541 mg, 13%. ^{1}H NMR ($CDCl_3$) δ 10.30 (s, 2 H, *meso*), 9.38 (d, $J = 5$ Hz, 4 H, β), 9.19 (d, $J = 4$ Hz, 2 H, β), 9.07 (d, $J = 5$ Hz, 2 H, β), 8.30 (d, $J = 8$ Hz, 2 H, Ar), 8.26 (d, $J = 8$ Hz, 2 H, Ar), 7.43 (d, $J = 3$ Hz, 1 H, Ar), 6.93 (t, $J = 3$ Hz, 2 H, Ar), 4.16 (t, $J = 7$ Hz, 4 H, octyloxy), 1.90 (t−t, $J = 7$ Hz, 4 H, octyloxy), 1.38−1.27 (m, 20 H, octyloxy), 0.88 (t, $J = 7$ Hz, 6 H, octyloxy), and −3.11 (s, 2 H, N−H); FAB MS *m*/*z* 844.1, calcd for $C_{54}H_{65}B_1N_4O_4$ *m*/*z* 844.5.

5,15-Dibromo-10-[4-(4,4,5,5-tetramethyl-1,3,2-dioxaborolan-2-yl)-phenyl]-20-(3,5-dioctyloxyphenyl)porphyrin Zinc(II) 2. The porphyrin **1** (200 mg, 0.237 mmol) was dissolved in a mixture of $CHCl_3$ (100 mL) and pyridine (0.5 mL). NBS (0.480 mmol) was added to this solution, and the resulting solution was stirred for 2 h at 0 °C. The mixture was poured into water and extracted with $CHCl_3$. The combined organic extracts were dried over anhydrous Na_2SO_4. A saturated solution of $Zn(OAc)_2$ in MeOH was added to the solution, and the resulting mixture was stirred for 2 h. The mixture was poured into water and extracted with $CHCl_3$. After the combined organic extracts were dried over Na_2SO_4, the solvent was removed by a rotary evaporator and the residue was purified by silica gel column chromatography with CH_2Cl_2. The product was recrystallized from $CHCl_3$−MeOH. Yield; 232 mg, 92%. ^{1}H NMR ($CDCl_3$) δ 9.70 (m, $J = 5$ Hz, 4 H, β), 9.05 (d, $J = 5$ Hz, 2 H, β), 8.91 (d, $J = 5$ Hz, 2 H, β), 8.21 (d, $J = 8$ Hz, 2 H, Ar), 8.17 (d, $J = 8$ Hz, 2 H, Ar), 7.32 (d, $J = 3$ Hz, 2 H, Ar), 6.90 (t,

(23) Ka, J.-W.; Lee, C.-H. *Tetrahedron Lett.* **2000**, *41*, 4609.

J = 3 Hz, 1 H, Ar), 4.13 (t, J = 7 Hz, 4 H, octyloxy), 1.88 (t−t, J = 7 Hz, 4 H, octyloxy), 1.38−1.26 (m, 20 H, octyloxy), and 0.87 (t, J = 7 Hz, 6 H, octyloxy); FAB MS m/z 1064.25, calcd for $C_{54}H_{61}B_1Br_2N_4O_4Zn$ m/z 1064.24.

5-[4-(4,4,5,5-Tetramethyl-1,3,2-dioxaborolan-2-yl)phenyl]-10,20-bis(phenylethynyl)-15-(3,5-dioctyloxyphenyl)porphyrin Zinc(II) 3. The bromoporphyrin **2** (200 mg, 0.19 mmol) and phenylacetylene (153 mg, 1.50 mmol) were dissolved in a mixture of dry toluene (20 mL) and triethylamine (4 mL), and this solution was purged with Ar for 30 min. $Pd(PPh_3)_2Cl_2$ (30 mg) and CuI (12 mg) were added, and the resulting solution was heated at 50 °C for 3 h under Ar. After the reaction mixture was filtered, the filtrate was separated by chromatography on a silica gel column (eluant CH_2Cl_2/n-hexane) to give **3**. The product was recrystallized from CH_2Cl_2−MeOH. Yield; 132 mg, 64%. ^{1}H NMR ($CDCl_3$) δ 9.70 (d, J = 5 Hz, 2 H, β), 9.69 (d, J = 5 Hz, 2 H, β), 9.04 (d, J = 5 Hz, 2 H, β), 8.89 (d, J = 5 Hz, 2 H, β), 8.22 (m, 4 H, Ar), 7.95 (d, J = 8 Hz, 4 H, Ph), 7.52 (t, J = 7 Hz, 4 H, Ph), 7.44 (t, J = 8 Hz, 2 H, Ph), 7.36 (d, J = 3 Hz, 2 H, Ar), 6.89 (t, J = 3 Hz, 1 H, Ar), 4.14 (t, J = 7 Hz, 4 H, octyloxy), 1.89 (t−t, J = 7 Hz, 4 H, octyloxy), 1.51−1.28 (m, 20 H, octyloxy), and 0.86 (t, J = 7 Hz, 6 H, octyloxy); FAB MS m/z 1106.6, calcd for $C_{70}H_{71}B_1N_4O_4Zn$ m/z 1106.5; UV−vis (THF) λ_{max} 448 and 648 nm.

General Procedure for Preparation of Z*n*A via Palladium-Catalyzed Cross-Coupling. Brominated *meso*−*meso* linked Zn(II) 5,-15-bis(3,5-dioctyloxyphenyl)porphyrin arrays, porphyrin boronate **3**, Cs_2CO_3 (1.5 equiv for **3**), and $Pd(PPh_3)_4$ (10 mol % for the bromoporphyrin) were dissolved in a mixture of dry DMF and toluene. The solution was deoxygenated three times via freeze−pump−thaw degas cycles, and the resulting mixture was heated at 80−90 °C for 3 h under Ar. At the endpoint, the reaction was quenched with water and extracted with ether. The organic layer was dried over anhydrous Na_2SO_4, passed through a short silica gel column, and evaporated. The product separation was performed on a preparative size exclusion column. Larger oligomers elute first, and then smaller oligomers were separated. Selected physical properties and detailed isolation procedures are presented below.

Z1A. A round-bottomed flask was charged with **3** (11 mg, 0.0099 mmol), 5-bromo-10,20-bis(3,5-dioctyloxyphenyl)porphyrin (5.0 mg, 0.0041 mmol), Cs_2CO_3, Pd-catalyst, dry toluene(2 mL), and dry DMF (1 mL). After the usual workup, the oligomers were separated by an SEC. Fractions of 2-mer and 1-mer were separated, and the solvent was removed by a rotary evaporator. The desired product was a dark green solid in 77% yield. ^{1}H NMR ($CDCl_3$) δ 10.32 (s, 1 H, *meso*), 10.00 (d, J = 5 Hz, 2 H, β), 9.84 (d, J = 5 Hz, 2 H, β), 9.47−9.45 (m, 4 H, β), 9.42 (d, J = 5 Hz, 2 H, β), 9.35 (d, J = 5 Hz, 2 H, β), 9.30 (d, J = 5 Hz, 2 H, β), 9.11 (d, J = 5 Hz, 2 H, β), 8.66 (d, J = 8 Hz, 2 H, Ar), 8.61 (d, J = 8 Hz, 2 H, Ar), 8.11 (d, J = 7 Hz, 4 H, Ph), 7.61 (t, J = 7 Hz, 4 H, Ph), 7.54−7.51 (m, 6 H, Ar + Ph), 7.42 (d, J = 3 Hz, 2 H, Ar), 6.97 (t, J = 3 Hz, 2 H, Ar), 6.94 (t, J = 3 Hz, 1 H, Ar), 4.21−4.19 (m, 12 H, octyloxy), 1.93−1.90 (m, 12 H, octyloxy), 1.51−1.27 (m, 60 H, octyloxy), and 0.87 (t, J = 7 Hz, 18 H, octyloxy); MALDI-TOF MS m/z 2020.7, calcd for $C_{128}H_{142}N_8O_6Zn_2$ m/z 2019.0; UV−vis (THF) λ_{max} 419, 448, 550, 590, and 650 nm; Fluorescence (THF, λ_{ex} = 550 nm) λ_{em} 654 and 716 nm.

Z2A. (76%) ^{1}H NMR ($CDCl_3$) δ 10.40 (s, 1 H, *meso*), 10.01 (d, J = 5 Hz, 2 H, β), 9.86 (d, J = 5 Hz, 2 H, β), 9.52 (d, J = 5 Hz, 2 H, β), 9.50 (d, J = 5 Hz, 2 H, β), 9.45 (d, J = 5 Hz, 2 H, β), 9.35 (d, J = 5 Hz, 2 H, β), 9.28 (d, J = 5 Hz, 2 H, β), 9.13 (d, J = 5 Hz, 2 H, β), 8.86 (d, J = 5 Hz, 2 H, β), 8.84 (d, J = 5 Hz, 2 H, β), 8.75 (d, J = 8 Hz, 2 H, Ar), 8.66 (d, J = 8 Hz, 2 H, Ar), 8.18 (d, J = 5 Hz, 2 H, β), 8.12−8.10 (m, 6 H, β + Ph), 7.61 (t, J = 7 Hz, 4 H, Ph), 7.54 (t, J = 8 Hz, 2 H, Ph), 7.50 (d, J = 3 Hz, 4 H, Ar), 7.44 (d, J = 3 Hz, 4 H, Ar), 7.43 (d, J = 3 Hz, 2 H, Ar), 6.95 (t, J = 3 Hz, 1 H, Ar), 6.85 (t, J = 3 Hz, 2 H, Ar), 6.82 (t, J = 3 Hz, 2 H, Ar), 4.19 (t, J = 7 Hz, 4 H, octyloxy), 4.10 (m, 16 H, octyloxy), 1.92 (t, J = 7 Hz, 4 H, octyloxy), 1.81 (t−t, J = 7 Hz, 16 H, octyloxy), 1.51−1.22 (m, 100 H, octyloxy), 0.88 (t, J = 7 Hz, 6 H, octyloxy), and 0.80 (t, J = 7 Hz, 24 H, octyloxy); MALDI-TOF MS m/z 3056.7, calcd for $C_{192}H_{224}N_{12}O_{10}Zn_3$ m/z 3055.5; UV−vis (THF) λ_{max} 423, 448, 465, 564, 604, and 649 nm; Fluorescence (THF, λ_{ex} = 564 nm) λ_{em} 655 and 716 nm.

Z3A. (37%) ^{1}H NMR ($CDCl_3$) δ 10.40 (s, 1H, *meso*), 10.00 (d, J = 5 Hz, 2 H, β), 9.87 (d, J = 5 Hz, 2 H, β), 9.54 (d, J = 5 Hz, 2 H, β), 9.51 (d, J = 5 Hz, 2 H, β), 9.48 (d, J = 5 Hz, 2 H, β), 9.38 (d, J = 5 Hz, 2 H, β), 9.30 (d, J = 5 Hz, 2 H, β), 9.14 (d, J = 5 Hz, 2 H, β), 8.93 (d, J = 5 Hz, 2 H, β), 8.91 (d, J = 5 Hz, 2 H, β), 8.86 (d, J = 5 Hz, 2 H, β), 8.82 (d, J = 5 Hz, 2 H, β), 8.77 (d, J = 8 Hz, 2 H, Ar), 8.69 (d, J = 8 Hz, 2 H, Ar), 8.28 (d, J = 5 Hz, 2 H, β), 8.26 (d, J = 5 Hz, 2 H, β), 8.23 (d, J = 5 Hz, 2 H, β), 8.15−8.12 (m, 6 H, β + Ph), 7.64 (t, J = 7 Hz, 4 H, Ph), 7.55 (t, J = 8 Hz, 2 H, Ph), 7.54 (d, J = 3 Hz, 4 H, Ar), 7.46 (d, J = 3 Hz, 4 H, Ar), 7.43 (d, J = 3 Hz, 2 H, Ar), 7.41 (d, J = 3 Hz, 4 H, Ar), 6.96 (t, J = 3 Hz, 1 H, Ar), 6.90 (t, J = 3 Hz, 2 H, Ar), 6.85 (t, J = 3 Hz, 2 H, Ar), 6.69 (t, J = 3 Hz, 2 H, Ar), 4.20 (t, J = 7 Hz, 4 H, octyloxy), 4.15−4.09 (m, 16 H, octyloxy), 3.98 (t, J = 7 Hz, 8 H, octyloxy), 1.93 (t−t, J = 7 Hz, 4 H, octyloxy), 1.84 (t−t, J = 7 Hz, 16 H, octyloxy), 1.71 (t−t, J = 7 Hz, 8 H, octyloxy), 1.55−1.15 (m, 140 H, octyloxy), and 0.92−0.72 (m, 42 H, octyloxy); MALDI-TOF MS m/z 4094.9, calcd for $C_{256}H_{306}N_{16}O_{14}Zn_4$ m/z 4092.9; UV−vis (THF) λ_{max} 418, 448, 480, 573, and 649 nm; Fluorescence (THF, λ_{ex} = 560 nm) λ_{em} 655 and 715 nm.

Z6A. (10%) ^{1}H NMR ($CDCl_3$) δ 10.41 (s, 1 H, *meso*), 10.03 (d, J = 5 Hz, 2 H, β), 9.87 (d, J = 5 Hz, 2 H, β), 9.56 (d, J = 5 Hz, 2 H, β), 9.52 (d, J = 5 Hz, 2 H, β), 9.48 (d, J = 5 Hz, 2 H, β), 9.40 (d, J = 5 Hz, 2 H, β), 9.30 (d, J = 5 Hz, 2 H, β), 9.14 (d, J = 5 Hz, 2 H, β), 8.96−8.90 (m, 18 H, β), 8.84 (d, J = 5 Hz, 2 H, β), 8.78 (d, J = 8 Hz, 2 H, Ar), 8.69 (d, J = 8 Hz, 2 H, Ar), 8.35−8.31 (m, 14 H, β), 8.28 (d, J = 5 Hz, 2 H, β), 8.26 (d, J = 5 Hz, 2 H, β), 8.16 (d, J = 5 Hz, 2 H, β), 8.13 (d, J = 8 Hz, 4 H, Ph), 7.64 (t, J = 7 Hz, 4 H, Ph), 7.56 (d, J = 3 Hz, 4 H, Ar), 7.55 (t, J = 8 Hz, 2 H, Ph), 7.49−7.48 (m, 16 H, Ar), 7.45 (d, J = 3 Hz, 4 H, Ar), 7.43 (d, J = 3 Hz, 2 H, Ar), 6.96 (t, J = 3 Hz, 1 H, Ar), 6.90 (t, J = 3 Hz, 2 H, Ar), 6.85 (t, J = 3 Hz, 2 H, Ar), 6.77−6.72 (m, 8 H, Ar), 4.20−4.04 (m, 52 H, octyloxy), 1.89−1.19 (m, 312 H, octyloxy), and 0.91−0.74 (m, 78 H, octyloxy); MALDI-TOF MS m/z 7203.8, calcd for $C_{448}H_{552}N_{28}O_{26}Zn_7$ m/z 7203.2; UV−vis (THF) λ_{max} 417, 448, 499, 582, and 649 nm; Fluorescence (THF, λ_{ex} = 560 nm) λ_{em} 654 and 717 nm.

Z12A. (34%) ^{1}H NMR ($CDCl_3$) δ 10.41 (s, 1H, *meso*), 10.03 (d, J = 5 Hz, 2 H, β), 9.87 (d, J = 5 Hz, 2 H, β), 9.56 (d, J = 5 Hz, 2 H, β), 9.52 (d, J = 5 Hz, 2 H, β), 9.48 (d, J = 5 Hz, 2 H, β), 9.40 (d, J = 5 Hz, 2 H, β), 9.30 (d, J = 5 Hz, 2 H, β), 9.14 (d, J = 5 Hz, 2 H, β), 8.96−8.90 (m, 42 H, β), 8.84 (d, J = 5 Hz, 2 H, β), 8.78 (d, J = 8 Hz, 2 H, Ar), 8.69 (d, J = 8 Hz, 2 H, Ar), 8.35−8.31 (m, 38 H, β), 8.28 (d, J = 5 Hz, 2 H, β), 8.26 (d, J = 5 Hz, 2 H, β), 8.16 (d, J = 5 Hz, 2 H, β), 8.13 (d, J = 8 Hz, 4 H, Ph), 7.64 (t, J = 7 Hz, 4 H, Ph), 7.56−7.48 (m, 52 H, Ar), 6.96 (t, J = 3 Hz, 1 H, Ar), 6.90 (t, J = 3 Hz, 2 H, Ar), 6.85 (t, J = 3 Hz, 2 H, Ar), 6.77−6.72 (m, 20 H, Ar), 4.20−4.04 (m, 100 H, octyloxy), 1.89−1.19 (m, 600 H, octyloxy), and 0.91−0.74 (m, 150 H, octyloxy); MALDI-TOF MS m/z 13423, calcd for $C_{832}H_{1044}N_{52}O_{50}Zn_{13}$ m/z 13423.9; UV−vis (THF) λ_{max} 415, 448, 506, 586, and 649 nm; Fluorescence (THF, λ_{ex} = 560 nm) λ_{em} 654 and 717 nm.

Z24A. (28%) ^{1}H NMR ($CDCl_3$) δ 10.42 (s, 1H, *meso*), 10.04 (d, J = 5 Hz, 2 H, β), 9.87 (d, J = 5 Hz, 2 H, β), 9.56 (d, J = 5 Hz, 2H, β), 9.52 (d, J = 5 Hz, 2 H, β), 9.48 (d, J = 5 Hz, 2 H, β), 9.40 (d, J = 5 Hz, 2 H, β), 9.30 (d, J = 5 Hz, 2 H, β), 9.14 (d, J = 5 Hz, 2 H, β), 8.96−8.90 (m, 90 H, β), 8.84 (d, J = 5 Hz, 2 H, β), 8.78 (d, J = 8 Hz, 2 H, Ar), 8.69 (d, J = 8 Hz, 2 H, Ar), 8.35−8.31 (m, 86 H, β), 8.28 (d, J = 5 Hz, 2 H, β), 8.26 (d, J = 5 Hz, 2 H, β), 8.16 (d, J = 5 Hz, 2 H, β), 8.13 (d, J = 8 Hz, 4H, Ph), 7.64 (t, J = 7 Hz, 4 H, Ph), 7.56−7.48 (m, 100 H, Ar), 6.96 (t, J = 3 Hz, 1 H, Ar), 6.90 (t, J = 3 Hz, 2 H, Ar), 6.85 (t, J = 3 Hz, 2 H, Ar), 6.77−6.72 (m, 44 H, Ar), 4.20−4.04 (m, 196 H, octyloxy), 1.89−1.19 (m, 1176 H, octyloxy), and 0.91−0.74 (m, 294 H, octyloxy); MALDI-TOF MS m/z 25862,

calcd for $C_{1600}H_{2028}N_{100}O_{98}Zn_{25}$ *m*/*z* 25865.1; UV−vis (THF) λ_{max} 415, 448, 509, 588, and 649 nm; Fluorescence (THF, λ_{ex} = 560 nm) λ_{em} 654 and 717 nm.

Acknowledgment. This work was supported by Grant-in-Aid for Scientific Research (No. 1123205 and No. 12440196). The work at Yonsei University was financially supported by the Creative Research Initiatives Program of the Ministry of Science and Technology of Korea. N.A. thanks the JSPS Research Fellowship for Young Scientists. We thank Ms. Victoria Browne for helpful discussions.

Supporting Information Available: The GPC chromatogram for **Z24A**, the absorption spectra and the fluorescence spectra of ***Zn*A** taken upon excitation with the absorbance adjusted, the transient absorption spectra at magic angle of **Z1A** and **Z2A**, and the steady-state fluorescence anisotropy spectra of **Z1A**−**Z6A**. This material is available free of charge via the Internet at http://pubs.acs.org.

JA030002U